nature medicine

17-AAG, an Hsp90 inhibitor, ameliorates polyglutamine-mediated motor neuron degeneration

Masahiro Waza[1,2], Hiroaki Adachi[1,2], Masahisa Katsuno[1], Makoto Minamiyama[1], Chen Sang[1], Fumiaki Tanaka[1], Akira Inukai[1], Manabu Doyu[1] & Gen Sobue[1]

Heat-shock protein 90 (Hsp90) functions as part of a multichaperone complex that folds, activates and assembles its client proteins. Androgen receptor (AR), a pathogenic gene product in spinal and bulbar muscular atrophy (SBMA), is one of the Hsp90 client proteins. We examined the therapeutic effects of 17-allylamino-17-demethoxygeldanamycin (17-AAG), a potent Hsp90 inhibitor, and its ability to degrade polyglutamine-expanded mutant AR. Administration of 17-AAG markedly ameliorated motor impairments in the SBMA transgenic mouse model without detectable toxicity, by reducing amounts of monomeric and aggregated mutant AR. The mutant AR showed a higher affinity for Hsp90-p23 and preferentially formed an Hsp90 chaperone complex as compared to wild-type AR; mutant AR was preferentially degraded in the presence of 17-AAG in both cells and transgenic mice as compared to wild-type AR. 17-AAG also mildly induced Hsp70 and Hsp40. 17-AAG would thus provide a new therapeutic approach to SBMA and probably to other related neurodegenerative diseases.

Hsp90, which accounts for 1–2% of cytosolic protein, is one of the most abundant cellular chaperone proteins[1]. It functions in a multicomponent complex of chaperone proteins including Hsp70, Hop (Hsp70 and Hsp90 organizing protein), Cdc37, Hsp40 and p23. Hsp90 is involved in the folding, activation and assembly of several proteins, known as Hsp90 client proteins[1]. As numerous oncoproteins have been shown to be Hsp90 client proteins[1], Hsp90 inhibitors have become a new strategy in antitumor therapy[2]. Geldanamycin, a classical Hsp90 inhibitor, is known as a potent antitumor agent[2]; however, it has not been used in clinical trials because of its liver toxicity[3]. 17-AAG is a new derivative of geldanamycin that shares its important biological activities[4] but shows less toxicity[5].

Hsp90 requires several interacting, co-chaperone proteins to exert its function on Hsp90 client proteins in Hsp90 complexes[1], of which two main forms exist[6]. One complex is a proteasome-targeting form associated with Hsp70 and Hop, and the other is a stabilizing form with Cdc37 and p23 (refs. 7,8). Particularly, p23 is thought to modulate Hsp90 activity in the last stages of the chaperoning pathway, leading to stabilized Hsp90 client proteins[9]. Hsp90 inhibitors, including 17-AAG, inhibit the progression of the Hsp90 complex toward the stabilizing form[10–12], and shift it to the proteasome-targeting form[7,8], resulting in enhanced proteasomal degradation of the Hsp90 client protein[7,13–18].

Because 17-AAG has less toxicity and higher selectivity for client oncoproteins[19], 17-AAG is now in clinical trials for a wide range of malignancies[20]. Additionally, Hsp90 inhibitors also function as Hsp inducers[20,21]. Several previous studies have suggested that Hsp90 inhibitors could be applied to nononcological diseases as neuroprotective agents based on their induction of Hsps[22–28].

Androgen receptor (AR) is one of the Hsp90 client proteins[15], and is a pathogenic gene product of spinal and bulbar muscular atrophy (SBMA), one of the polyglutamine (polyQ) diseases[29]. This disease is characterized by premature muscular exhaustion, slow progressive muscular weakness, atrophy and fasciculation in bulbar and limb muscles[30]. PolyQ diseases are inherited neurodegenerative disorders caused by the expansion of a trinucleotide CAG repeat in the causative genes[31]. In SBMA, the number of polymorphic CAG repeats is normally 14–32, whereas it is expanded to 40–62 CAGs in the *AR* gene[32]. A correlation exists between CAG repeat size and disease severity[33]. The pathologic features of SBMA are motor neuron loss in the spinal cord and brainstem[30], and diffuse nuclear accumulation and nuclear inclusions of the mutant AR in the residual motor neurons and certain visceral organs[34].

We have already examined several therapeutic approaches in a mouse model of SBMA[35–38]. As a consequence, we confirmed that castration and leuprorelin, a luteinizing hormone–releasing hormone agonist that reduces testosterone release from the testis, substantially rescued motor dysfunction and nuclear accumulation of mutant AR in male transgenic mice[35,37]. Although this hormonal therapy was effective, it poses the unavoidable difficulty of severe sexual dysfunction[37]. In addition, this therapy cannot be applied to other polyQ diseases.

Here, we present a new and potent strategy for SBMA therapy with 17-AAG, an Hsp90 inhibitor. Given that Hsp90 inhibitors have two major activities, preferential client protein degradation and Hsp induction, we hypothesized that 17-AAG would degrade mutant AR more effectively than wild-type AR.

[1]Department of Neurology, Nagoya University Graduate School of Medicine, 65 Tsurumai-cho, Showa-ku, Nagoya 466-8550, Japan. [2]These authors contributed equally to this work. Correspondence should be addressed to G.S. (sobueg@med.nagoya-u.ac.jp).

Received 25 February; accepted 10 August; published online 11 September 2005; doi:10.1038/nm1298

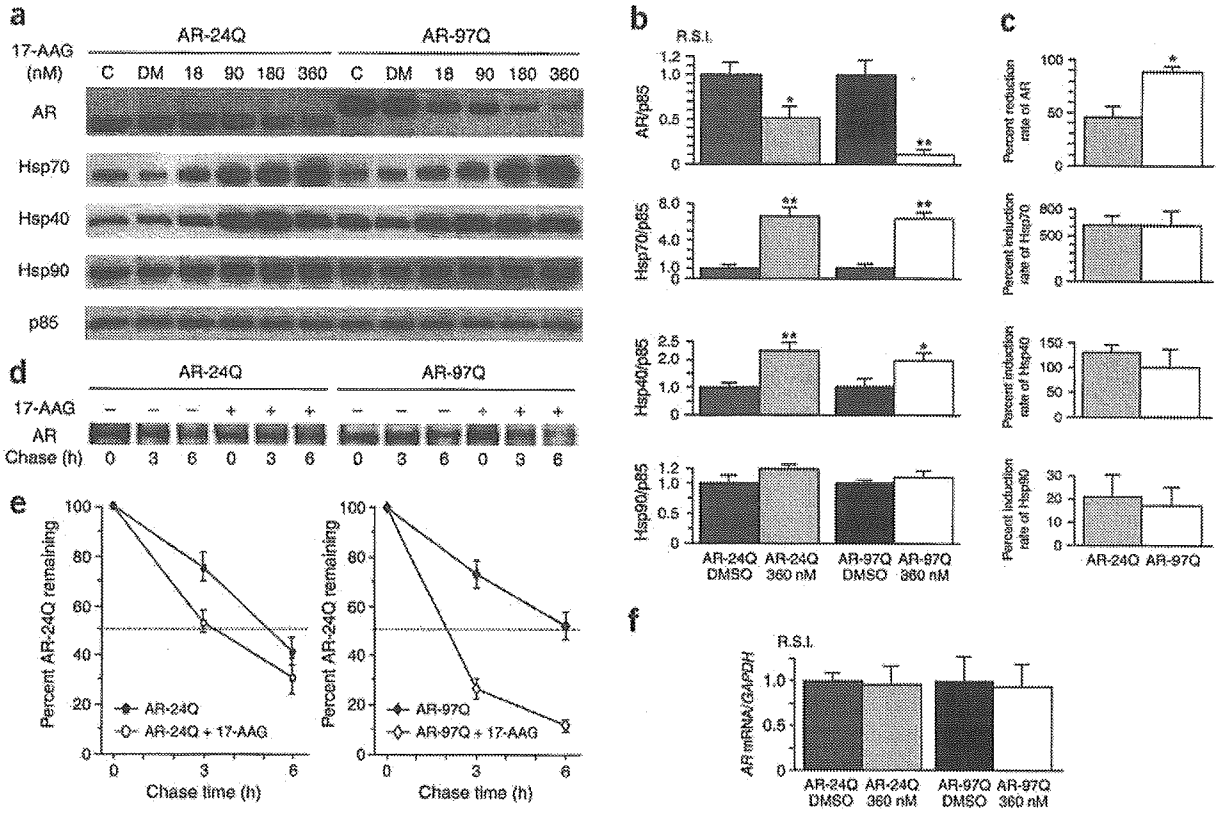

Figure 1 Effect of 17-AAG on the AR or chaperones in cultured-cell models. (**a**,**b**) Although the immunoblot and densitometric analysis showed a dose-dependent decline in both wild-type (AR-24Q) and mutant (AR-97Q) AR expression in response to 17-AAG, the mutant AR decreased more than did the wild-type. 17-AAG markedly increased the expression of Hsp70 and Hsp40, especially for Hsp70, but only slightly increased Hsp90 expression. (**c**) The decrease in mutant AR after treatment with 17-AAG was much higher than that of wild-type AR (88.9% versus 45.9%, $P = 0.0063$). Values are expressed as mean ± s.e.m. ($n = 5$). (**d**) Pulse-chase analysis of two forms of AR. Data from one representative experiment for wild-type and mutant AR. (**e**) Pulse-chase assessment of the half-life of wild-type and mutant AR. The amounts of AR-24Q and AR-97Q remaining in the absence and presence of 17-AAG are indicated. Values are expressed as mean ± s.e.m. ($n = 4$). (**f**) Real-time RT-PCR of wild-type and mutant *AR* mRNA. Quantities are shown as the ratio to *GAPDH* mRNA. The wild-type and mutant *AR* mRNA levels were similar under 17-AAG treatments. Values are expressed as mean ± s.e.m. ($n = 4$). $^{*}P < 0.025$, $^{**}P < 0.005$.

In this study, we examine the effects of 17-AAG on a cultured-cell model and the transgenic mouse model of SBMA. We show that the mutant AR exists more frequently as a stabilized Hsp90 chaperone complex than does the wild-type AR, and that 17-AAG selectively degrades the mutant AR. Administration of 17-AAG inhibits neuronal nuclear accumulation of the mutant AR and considerably ameliorates motor phenotypes of the SBMA model mouse.

RESULTS

Effect of 17-AAG on expression of AR and Hsps *in vitro*

To address the question of whether 17-AAG promotes the degradation of polyQ-expanded AR, we treated SH-SY5Y cells highly expressing the wild-type (AR-24Q) or mutant (AR-97Q) AR for 48 h with the indicated doses of 17-AAG or with DMSO as control. Although immunoblot analysis showed a dose-dependent decline in both wild-type and mutant AR expression after treatment with 17-AAG (**Fig. 1a**), the monomeric mutant AR decreased significantly more than did the wild-type ($P = 0.0063$; **Fig. 1b,c**), suggesting that the mutant AR is more sensitive to 17-AAG than is the wild-type. The expression of Hsp70 and Hsp40 were also markedly increased after treatment with 17-AAG, but Hsp90 was only slightly increased (**Fig. 1a,b**). There were no significant differences, however, in the levels of Hsp70, Hsp40 and Hsp90 induction between the wild-type and mutant AR (**Fig. 1c**).

To determine whether the decrease in AR resulted from protein degradation or from changes in RNA expression, we assessed the turnover of wild-type and mutant AR with a pulse-chase labeling assay. Without treatment, the wild-type and mutant AR were degraded in a similar manner, as previously reported[39,40]. In the presence of 17-AAG, however, the wild-type and mutant AR had half-lives of 3.5 h and 2 h, respectively (**Fig. 1d,e**), whereas levels of mRNA encoding the wild-type and mutant AR were quite similar (**Fig. 1f**). Cell viability did not differ between wild-type and mutant AR transfected cells (data not shown). These data indicate that 17-AAG preferentially degrades the mutant AR protein without cellular toxicity or alteration of mRNA levels.

To address why 17-AAG preferentially degrades mutant AR, we determined the levels of Hsp90, Hop and p23 associated with wild-type or mutant AR in SH-SY5Y cells without 17-AAG treatment (**Fig. 2a**). Hop and p23 are two essential components of multi-chaperone Hsp90 complexes[1]. Without 17-AAG treatment, coimmunoprecipitation from the cell lysates with antibodies to AR showed that p23 was more highly associated with mutant than with wild-type AR (**Fig. 2a,b**). The total levels of Hsp90, Hop and p23 were similar in the cells transfected with either wild-type or mutant AR (**Fig. 2a**).

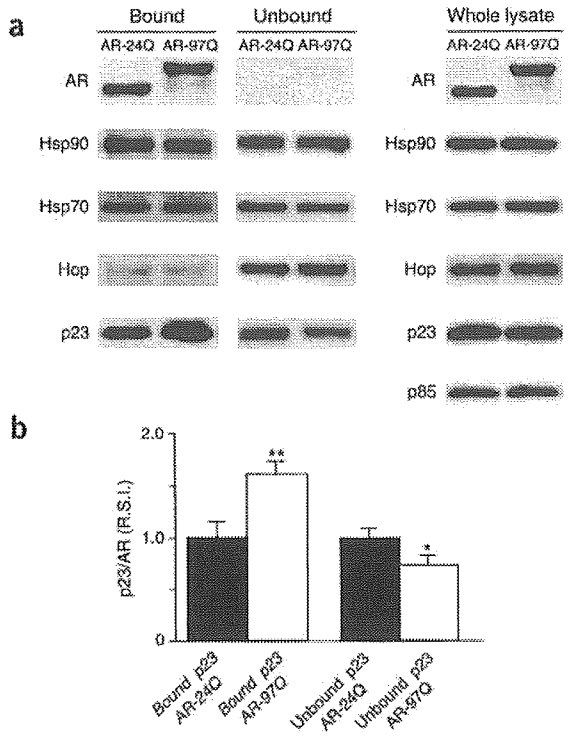

Figure 2 Immunoprecipitation of wild-type and mutant AR in cultured-cell models. (**a**) Wild-type and mutant AR were immunoprecipitated from cell lysates with an AR-specific antibody and immunoblotted with antibodies to the indicated western blot proteins. There was more mutant AR present in multichaperone complexes with p23 than there was wild-type AR. There were no differences in total expression levels of AR, Hsp90, Hsp70, Hop and p23 between wild-type and mutant AR–expressing cells. Control immunoprecipitations without antibodies did not immunoprecipitate any co-chaperones (data not shown). (**b**) The densitometric analysis of p23 in the bound and unbound fractions shows there was 1.6 times as much p23 associated with mutant AR than there was with the wild-type ($P < 0.01$). This experiment was repeated with five sets of cells with equivalent results. Values are expressed as mean ± s.e.m. ($n = 5$). $^{*}P < 0.05$, $^{**}P < 0.01$. R.S.I., relative signal intensity.

We next examined the status of the Hsp90 chaperone complex in wild-type and mutant AR-expressing cultured cells treated with 17-AAG. Immunoprecipitation with AR-specific antibody showed that Hsp90 chaperone complex–associated Hop was markedly increased, and p23 decreased depending on the dose of 17-AAG (**Fig. 3a,b**), suggesting that treatment with 17-AAG resulted in the shifting of the AR-Hsp90 chaperone complex from a mature stabilizing form with p23 to a proteasome-targeting form with Hop. The loss of p23 from the mutant AR-Hsp90 complex was significantly higher ($P < 0.005$) than that from the wild-type AR-Hsp90 complex (**Fig. 3c**). The degradation of wild-type and mutant AR by 17-AAG was completely blocked by the proteasome inhibitor MG132 (**Fig. 3d**), suggesting that the pharmacological degradation by 17-AAG was dependent on the proteasome system, as previously reported[17,18]. Furthermore, these results strongly suggest that mutant AR is more likely to be in the Hsp90-p23 multichaperone complexes, which eventually enhances 17-AAG–dependent proteasomal degradation of mutant AR.

Moreover, mutant AR was markedly decreased after treatment with 17-AAG even when induction of Hsp70 and Hsp40 was blocked by the protein-synthesis inhibitor cycloheximide (**Supplementary Fig. 1** online), suggesting that 17-AAG contributes to the preferential degradation of mutant AR mainly through Hsp90 chaperone complex formation and subsequent proteasome-dependent degradation rather than through induction of Hsp70 and Hsp40.

17-AAG ameliorates phenotypic expression of SBMA mice

We administered 17-AAG (2.5 or 25 mg/kg) to male transgenic mice carrying full-length human AR-24Q or AR-97Q. The disease progression of AR-97Q mice treated with 25 mg/kg 17-AAG (Tg-25) was

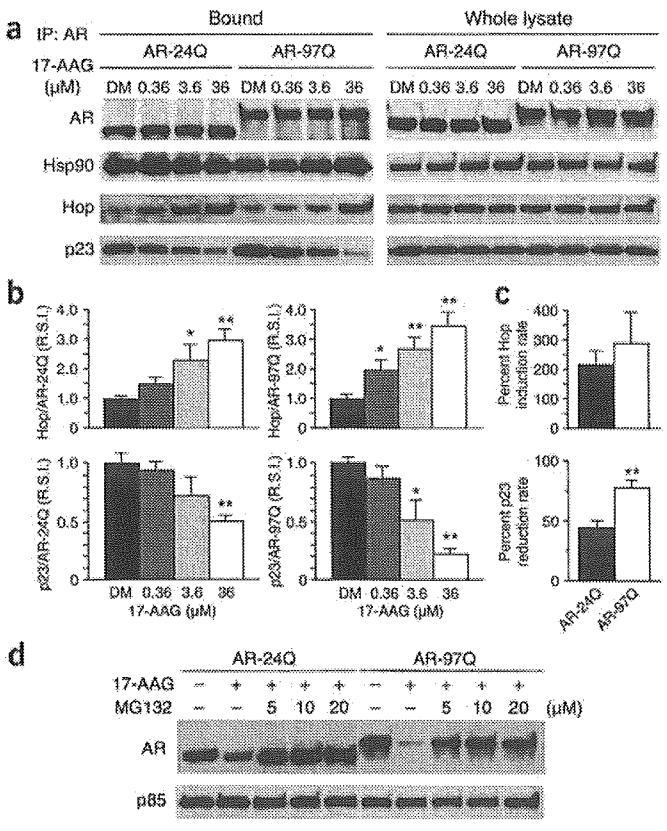

Figure 3 Pharmacological change in the AR-Hsp90 complex, and the correlation to proteasomal degradation. (**a**) Immunoblots of lysates of transfected cells treated with 17-AAG. Lysates were immunoprecipitated with AR-specific antibody. The short time exposure to 17-AAG did not decrease the amount of mutant AR. There were dose-dependent changes in both Hop and p23 after treatment with 17-AAG; however, no dissociation of Hsp90 from the mutant AR complex was seen. There were no changes in the expression of Hop, p23 and Hsp90 in whole lysates in the presence of 17-AAG. (**b**) Densitometric analysis of Hop and p23 in the bound fractions. There was a marked increase in the amount of Hop, and a marked decrease in p23 in both wild-type and mutant AR-bound Hsp90 complexes after treatment with 17-AAG. R.S.I., relative signal intensity. (**c**) Comparisons of induction rate of Hop and reduction rate of p23 in the Hsp90 complexes of wild-type and mutant AR. Although there was no significant difference in the induction rate of Hop between the wild-type and mutant AR complexes, the reduction rate of p23 was significantly higher in the mutant AR complex compared with that in the wild-type complex (43.8% versus 79.0%, $P < 0.005$). Values are expressed as means ± s.e.m. ($n = 5$). (**d**) Effect of 17-AAG on AR expression under the inhibition of proteasomal degradation. The mutant AR was more markedly reduced than wild-type AR after 17-AAG treatments; however, this pharmacological degradation was completely blocked by MG132 in both cases. DM, DMSO. $^{*}P < 0.025$, $^{*}P < 0.005$.

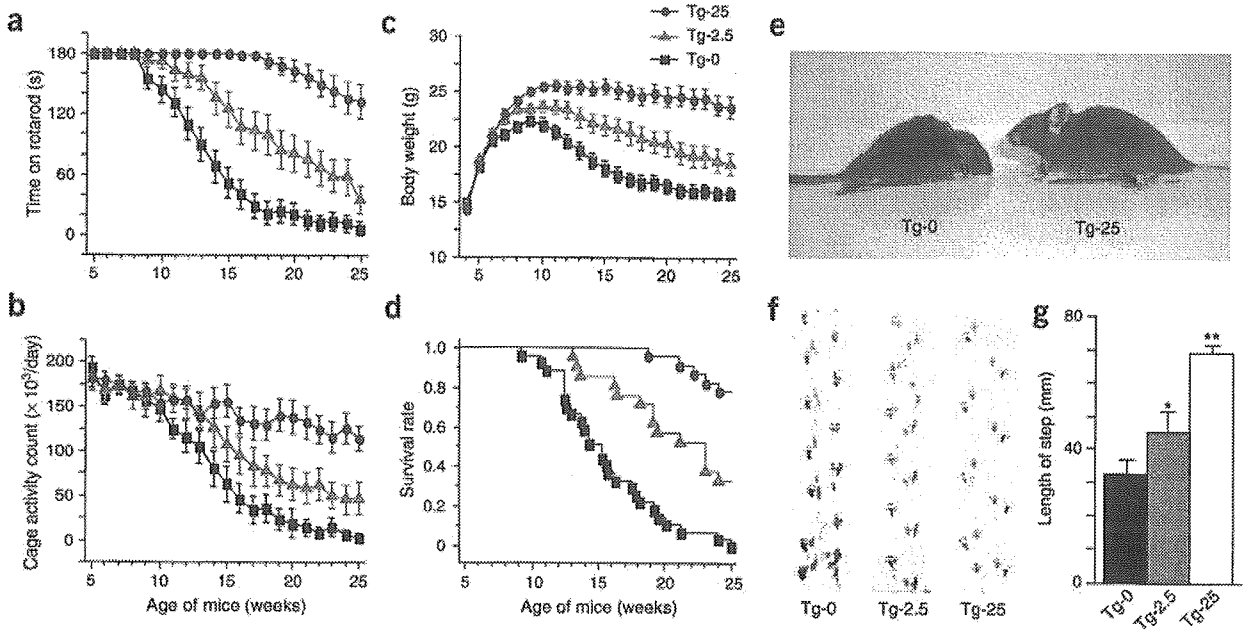

Figure 4 Effects of 17-AAG on behavioral and visible phenotypes in male AR-97Q mice. (**a**) Rotarod task ($n = 27$), (**b**) cage activity ($n = 18$), (**c**) body weight ($n = 27$) and (**d**) survival rate ($n = 27$) of Tg-0, Tg-2.5 and Tg-25 mice. All parameters were significantly different between the Tg-0 and Tg-25 ($P < 0.005$ for all parameters). A Kaplan-Meier plot shows the prolonged survival of Tg-2.5 and Tg-25 compared with Tg-0, which had all died by 25 weeks of age ($P = 0.004$, $P < 0.001$, respectively). (**e**) Representative photographs of a 16-week-old Tg-0 (left) shows an obvious difference in size, and illustrates muscular atrophy and kyphosis compared with an age-matched Tg-25 (right). (**f**) Footprints of representative 16-week-old Tg-0, Tg-2.5 and Tg-25 mice. Front paws are indicated in red and hind paws in blue. (**g**) The length of steps was measured in 16-week-old Tg-0, Tg-2.5 and Tg-25 mice. Each column shows an average of steps of the hind paw. Values are expressed as means ± s.e.m. ($n = 6$). $^*P < 0.025$, $^{**}P < 0.005$.

markedly ameliorated, and that of mice treated with the 2.5 mg/kg 17-AAG (Tg-2.5) was mildly ameliorated (**Fig. 4a–d**). The untreated transgenic male mice (Tg-0) showed motor impairment assessed by the rotarod task as early as 9 weeks after birth, whereas Tg-25 mice showed initial impairment only 18 weeks after birth and with less deterioration than Tg-0 mice (**Fig. 4a**). Tg-2.5 mice showed intermediate levels of impairment in rotarod performance (**Fig. 4a**). The locomotor cage activity of Tg-0 mice was also markedly decreased at 10 weeks compared with the other two groups, which showed decreases in activity at 13 (Tg-2.5) and 16 (Tg-25) weeks of age (**Fig. 4b**). Tg-0 mice lost weight significantly earlier and more profoundly than the Tg-2.5 ($P < 0.025$) and Tg-25 mice ($P < 0.005$; **Fig. 4c**). Treatment with 17-AAG also significantly prolonged the survival rate of Tg-2.5 ($P = 0.004$) and Tg-25 mice ($P < 0.001$) as compared to Tg-0 mice (**Fig. 4d**). 17-AAG was less effective at the close of 2.5 mg/kg than 25 mg/kg in all parameters tested. The lines were not distinguishable in terms of body weight at birth; however, by 16 weeks, Tg-0 mice showed obvious differences in body size, muscular atrophy and kyphosis compared to Tg-25 mice (**Fig. 4e**). Additionally, Tg-0 mice showed motor weakness, with short steps and dragging of the legs, whereas Tg-25 mice showed almost normal ambulation (**Fig. 4f,g**).

When we immunohistochemically examined mouse tissues for mutant AR using the 1C2 antibody, which specifically recognizes expanded polyQ, we observed a marked reduction in 1C2-positve nuclear accumulation in the spinal motor neurons (**Fig. 5a**) and muscles (**Fig. 5b**) of Tg-25 mice compared with those of Tg-0 mice. Glial fibrillary acidic protein (GFAP)-specific antibody staining showed an apparent reduction of reactive astrogliosis in Tg-25 compared with Tg-0 mice in the spinal anterior horn (**Fig. 5c**). Muscle histology also showed marked amelioration of neurogenic muscle atrophy in the AR-97Q mice treated with 17-AAG (**Fig. 5d**). We confirmed a significant reduction of 1C2-positive nuclear accumulation in both spinal cord ($P < 0.01$) and skeletal muscle ($P < 0.05$) by quantitative assessment (**Fig. 5e**). AR-24Q mice and normal littermates treated with 17-AAG showed no altered phenotypes (data not shown).

To evaluate the toxic effects of 17-AAG, we examined blood samples from 25-week-old mice treated with 25 mg/kg 17-AAG for 20 weeks. Measurements of aspartate aminotransferase, alanine aminotransferase, blood urea nitrogen and serum creatinine showed that treatment with 17-AAG resulted in neither infertility nor liver or renal dysfunction in the AR-97Q male mice at the dose of 25 mg/kg (**Supplementary Fig. 2** online).

Mutant AR is preferentially degraded by 17-AAG *in vivo*

As the mutant AR was preferentially degraded as compared to the wild-type AR in the presence of 17-AAG *in vitro*, we also examined the level of AR in the SBMA mouse model. Western blot analysis of lysates of the spinal cord and muscle of AR-97Q mice showed high molecular-weight mutant AR protein complex retained in the stacking gel as well as a band of monomeric mutant AR, whereas only the band of wild-type monomeric AR was visible in tissues from the AR-24Q mice (**Fig. 6a,b**). Treatment with 17-AAG notably diminished both the high molecular-weight complex and the monomer of mutant AR in the spinal cord and muscle of the AR-97Q mice, but only slightly diminished the wild-type monomeric AR in AR-24Q mice (**Fig. 6a,b**). Treatment with 17-AAG decreased the amount of the monomeric AR in AR-97Q mice by 64.4% in the spinal cord and 45.0% in the skeletal muscle, whereas these amounts were only 25.9% and 12.5%, respectively, in AR-24Q mice (**Fig. 6a,b**). Thus, the reduction rate of the monomeric mutant AR was significantly higher than the wild-type

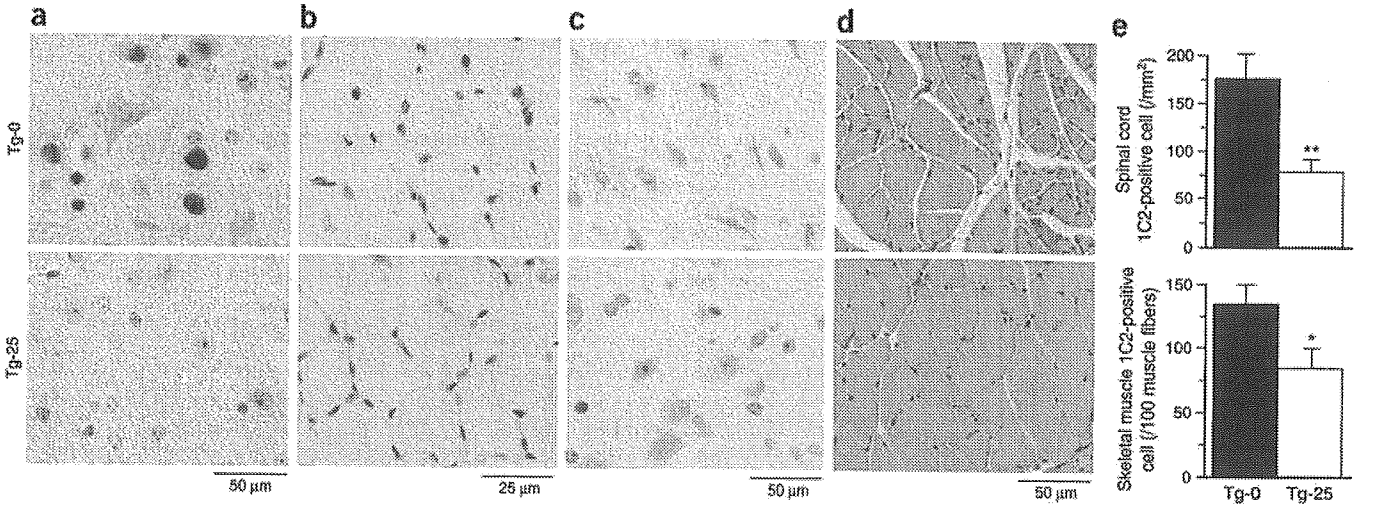

Figure 5 Effects of 17-AAG on the histopathology of male AR-97Q mice. (**a**,**b**) Immunohistochemical staining with 1C2-specific antibody showed marked differences in diffuse nuclear staining and nuclear inclusions between Tg-0 and Tg-25 mice in the spinal anterior horn and skeletal muscle, respectively. (**c**) Immunohistochemical staining with GFAP-specific antibody also showed an obvious reduction of reactive astrogliosis in the spinal anterior horn of mice treated with 17-AAG. (**d**) Hematoxylin and eosin staining of the muscle in Tg-0 mice showed obvious grouped atrophy and small angulated fibers, which were not seen in Tg-25 mice. (**e**) There was a significant reduction in 1C2-positive cell staining in the spinal cord ($P < 0.01$) and skeletal muscle ($P < 0.05$) in Tg-25 as compared to Tg-0 mice. Values are expressed as mean ± s.e.m. ($n = 6$). $^*P < 0.05$, $^{**}P < 0.01$.

AR in both spinal cord ($P < 0.001$) and skeletal muscle ($P < 0.01$; **Fig. 6c**). The levels of wild-type and mutant *AR* mRNA were similar in the respective mice treated with 17-AAG (**Fig. 6d**). We also performed filter-trap assays for quantitative analyses of both the large molecular aggregated and soluble forms of the mutant AR[36]. Both forms of trapped AR-97Q protein were markedly reduced in the spinal cord and muscle of Tg-25 mice, whereas those from the AR-24Q were not (**Supplementary Fig. 3** online). These observations strongly indicate that 17-AAG markedly reduces not only the monomeric mutant AR protein but also the high molecular–weight mutant AR complex, because of the preferential degradation of the mutant AR.

Western blot analysis showed that the levels of Hsp70 and Hsp40 in spinal cord were increased by 47.1% and 29.5%, respectively, and in muscle by 29.2% and 24.7%, respectively (**Supplementary Fig. 4** online) after treatment with 17-AAG. These pharmacological effects of chaperone induction were statistically significant ($P < 0.05$ for all parameters), but not as marked as the 17-AAG–induced mutant AR reduction, and were also not as pronounced as those arising from genetic manipulation in our previous study[36].

Hsp90 inhibitors nonspecifically activate heat shock responses through a dissociation of the heat-shock transcription factor (HSF-1) from the Hsp90 complex[27,41]. Although the expression of

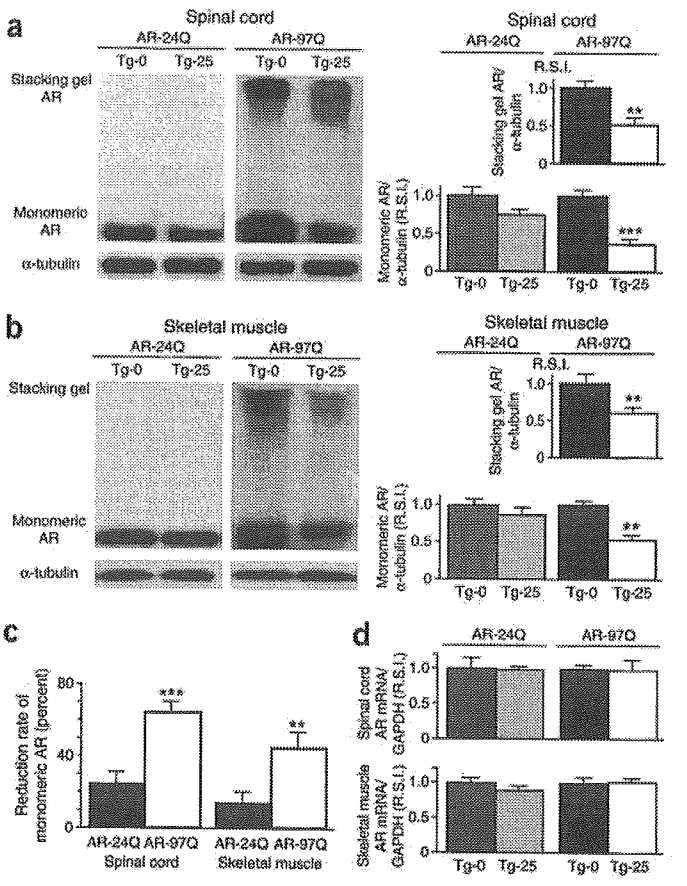

Figure 6 Effects of 17-AAG on AR expression in male AR-24Q or 97Q mice. (**a**,**b**) Western blot analysis of the spinal cord and muscle of AR-24Q and AR-97Q mice probed with AR-specific antibody. In both spinal cord and muscle of mice treated with 17-AAG, there was a significant decrease in the amount of mutant AR in the stacking gel and monomeric mutant AR in AR-97Q mice, but only slightly less monomeric wild-type AR in AR-24Q mice compared with that from untreated control mice. (**c**) Comparison of reduction rate of wild-type and mutant AR. Densitometric analysis showed that the 17-AAG–induced reduction of monomeric mutant AR was significantly greater than that of the wild-type monomeric AR. 17-AAG resulted in a 64.4% decline in monomeric mutant AR in the spinal cord, and a 45.0% decline in the skeletal muscle, whereas there was only a 25.9% decline in the spinal cord and a 12.5% decline in the skeletal muscle of AR-24Q mice. These results show significant differences of the reduction rate between wild-type and mutant AR in both spinal cord and skeletal muscle. Values are expressed as mean ± s.e.m. ($n = 5$). $^*P < 0.05$, $^{**}P < 0.01$, $^{***}P < 0.001$. (**d**) Real-time RT-PCR of wild-type and mutant *AR* mRNA *in vivo*. The expression levels of wild-type and mutant *AR* mRNA in transgenic mouse spinal cord and skeletal muscle were similar under 17-AAG treatments. Values are expressed as mean ± s.e.m. ($n = 3$).

Hsp90 and HSF-1 was not altered after 17-AAG treatment, coimmunoprecipitation of HSF-1 with Hsp90 in the spinal cord and skeletal muscle was significantly reduced ($P < 0.01$ for both) after 17-AAG treatment (**Supplementary Fig. 4** online), indicating that this drug induces Hsps through activation of HSF-1.

DISCUSSION

Our study showed that the polyQ-expanded mutant AR present in SBMA was preferentially degraded by treatment with 17-AAG. Elimination of mutant AR was mediated through its preferential incorporation into the Hsp90-chaperone complex, where it is then prone to proteasomal degradation. Owing to this mechanism, 17-AAG markedly ameliorated motor phenotypes of the SBMA mouse model without toxicity. Our present data from the mouse model also confirmed that 17-AAG passes through the blood-brain barrier as previously reported[42], and that it reaches a concentration high enough to have effects in the central nervous system.

Recently, some antitumor agents have been therapeutically applied to neurodegenerative diseases[43,44]. Most antitumor agents have some cytotoxic effects on normal cells, which must be overcome in any clinical application against neurodegeneration. Because neurodegenerative diseases generally follow a chronic progression and the medical treatment is, thus, long-standing compared to that for malignancy, the toxic side effects should be extensively suppressed. In contrast to general antitumor agents, the effects of 17-AAG have been known to have a high selectivity for tumor cells. This selectivity results from the high affinity of 17-AAG for the Hsp90 client oncoproteins when they are incorporated in the Hsp90-dependent multichaperone complex, thereby increasing their binding affinity for 17-AAG more than 100-fold[19]. This high selectivity of 17-AAG for the incorporated Hsp90 client protein eventually minimizes its toxic side effects and renders it very feasible for clinical applications, especially for neurodegenerative diseases. In fact, our transgenic mice were free from obvious side effects after the consecutive administration of 17-AAG for 20 weeks.

The major pharmacological effect of 17-AAG is to promote the dissociation of p23 from Hsp90 client protein complexes[10–12,16]. In this study, we showed that the mutant AR with an expanded polyQ had a higher association with p23 than did the wild-type AR. We consider this significantly higher association between the mutant AR and p23, particularly compared with the wild-type AR, to be the essential basis for preferential degradation of the polyQ-expanded mutant AR after 17-AAG treatment. Furthermore, the increase in Hop and decrease in p23 in the mutant AR-bound Hsp90 complex after 17-AAG treatment strongly supports the view that Hsp90 complexes were shifted to the proteasome-targeting form by 17-AAG, leading to proteasomal degradation of mutant AR. Given that the increase in Hop proteins in Hsp90 complexes and the decrease in p23 were only detected after the higher concentration of 17-AAG and after a very short period of incubation, this chaperone complex shift seems to be very rapid, as has been suggested previously[12].

Hsps, particularly Hsp70, have been shown to suppress aggregate formation and cellular toxicity in a wide range of polyQ disease models[21,36,45,46]. Geldanamycin has been considered a neuroprotective agent because of its ability to induce Hsp70 (refs. 22–24,27), and in polyQ diseases, has been proven to suppress aggregation of mutant huntingtin protein in a cultured-cell model through the induction of Hsp70 and Hsp40 (refs. 22,23). Hsp90 inhibitors have also been shown to be effective in animal models of Parkinson disease[24], stroke[27] and autoimmune encephalomyelitis[28]. It was thought that these effects were based only on the ability of the Hsp90 inhibitors to induce Hsps. As shown in this study, however, 17-AAG induced only limited amounts of Hsp70 and Hsp40 *in vivo*. Furthermore, our results suggest that the pathway for mutant AR degradation by 17-AAG through the Hsp90-client protein complex system is predominant. 17-AAG is expected to exert the most effective therapeutic potential for diseases in which the disease-causing protein belongs to the Hsp90 client protein family.

Mutant p53, which is present in nearly half of all malignancies and is an Hsp90 client protein, shows a much higher sensitivity to Hsp90 inhibitors than does wild-type p53 (ref. 47), just as AR, in its polyQ-expanded mutant form, acquired higher sensitivity to the Hsp90 inhibitor. In the case of neurodegenerative diseases, phosphorylated tau would be one of the target proteins of Hsp90 inhibitors, because geldanamycin substantially reduces the total amount of phosphorylated tau[25,26], and also inhibits tau aggregation[25]. According to these previous reports, our data suggest that 17-AAG would also be a candidate for a therapeutic approach to a wide range of tauopathies. The successful application of 17-AAG to polyQ diseases other than SBMA remains to be seen. But, as a previous report showed, the blockage of pathogenetic gene expression could reversibly reduce nuclear inclusions and reactive gliosis in a mouse model of Huntington disease by self-cleaning functions[48]. Indeed, one therapeutic approach, which directly reduced abnormal protein using RNA interference, proved to be beneficial in a mouse model of SCA1 (ref. 49). There is no doubt that the reduction of disease-causing protein would be beneficial in polyQ diseases. Therefore, once it is proven that the disease-causing proteins belong to the Hsp90 client protein family and have high affinities to Hsp90 inhibitors, 17-AAG is expected to preferentially degrade the expanded polyQ-containing disease proteins and, thus, would be a good candidate for clinical therapeutics.

In conclusion, we have shown the efficacy and safety of 17-AAG in a model mouse of SBMA, a neurodegenerative disease, and considerably extended the therapeutic application of 17-AAG beyond oncological diseases. In addition, we have documented the differential degradation efficacy of a polyQ-expanded mutant protein compared with its wild-type form. This strategy is apparently different from the previous strategy for polyQ diseases, which unavoidably allowed abnormal protein to remain and placed much value mainly on the inhibition of protein aggregation. 17-AAG, directly reducing disease-causing protein itself, presents a new therapeutic avenue for SBMA, and has potentially widespread application for other neurodegenerative diseases.

METHODS

DNA transfection. We constructed full-length ARs by subcloning AR inserts derived from pSP64-AR24 or pSP64-AR97 (ref. 46) into the pCR3.1 mammalian expression vector (Invitrogen). We plated SH-SY5Y cells in 6-cm dishes and transfected each dish with 8 μg of the vector containing AR24 or AR97 using Lipofectamine 2000 (Invitrogen) according to the manufacturer's instructions. We cultured the cells for 48 h. In this culture system, we detected a band of monomeric mutant AR in the separating gel, but could hardly detect the high molecular–weight mutant AR protein complex, which was retained in the stacking gel.

Neurological and behavioral assessment of SBMA model mice. We generated and maintained the AR-24Q and AR-97Q mice as previously described[35] (**Supplementary Methods** online). All animal experiments were performed in accordance with the National Institutes of Health Guide for the Care and Use of Laboratory Animals and under the approval of the Nagoya University Animal Experiment Committee. We performed the mouse rotarod task and cage activity as described previously[35]. The investigators in the behavioral assessment were blinded to the treatments.

Therapeutic agents and protocol for administration. We obtained 17-AAG, also known as NSC 330507, from the Regulatory Affairs Branch, Division of

Cancer Treatment and Diagnosis, National Cancer Institute and Kosan Biosciences. For cultured-cell models, we diluted a 1.8 mM stock solution of 17-AAG in DMSO into fresh medium to give final concentrations of 18–360 nM. In the cycloheximide study, we treated cells for 48 h with 17-AAG in the presence of 5 μg/ml cycloheximide (Sigma). To show pharmacological changes in the AR-Hsp90 complex, we exposed cultured cells for 30 min to 17-AAG at concentrations of 0.36, 3.6 and 36 μM 48 h after transfection. In the proteasome-inhibitory study, we exposed cultured cells for 6 h to 36 μM 17-AAG, and 5, 10 and 20 μM MG132 (Sigma) beginning 48 h after transfection.

For mouse models, we stored 50 mg/ml stock solutions of 17-AAG dissolved in DMSO at –20 °C. We began 17-AAG treatments when mice attained the age of 5 weeks, and continued them until mice were 25 weeks old. Normal male littermates, AR-24Q mice and AR-97Q mice received 50 μl intraperitoneal injections of 2.5 or 25 mg/kg 17-AAG three times a week on alternate days; control mice received DMSO alone.

Protein expression analysis. We lysed cells in CelLytic-M Mammalian Cell Lysis/Extraction Reagent (Sigma) and centrifuged them at 15,000*g* for 15 min at 4 °C. We homogenized the tissues from 16-week-old mice in CelLytic-M (Sigma) and centrifuged them at 2,500*g* for 15 min at 4 °C. Primary antibodies were as follows: AR-specific antibody (N-20 or H280; Santa Cruz); Hsp70-specific antibody (SPA-810; Stressgen); Hsp40-specific antibody (SPA-400; Stressgen); Hsp90-specific antibody (SPA-835; Stressgen); Hop-specific antibody (SRA-1500; Stressgen); p23-specific antibody (MA3-414; Affinity BioReagents); HSF-1–specific antibody (SPA-901; Stressgen); p85-specific antibody (Upstate); and α-tubulin–specific antibody (T9026; Sigma). We used the LAS-3000 imaging system to produce digital images and to quantify band intensities, which we then analyzed with Image Gauge software version 4.22 (Fujifilm). Densitometric values of AR, Hsp70, Hsp40 and Hsp90 were normalized to those of endogenous p85 or α-tubulin. Relative signal intensity (R.S.I.) was computed as the signal intensity of each sample divided by that of DMSO-treated cells or DMSO-treated mice.

We performed immunoprecipitation from cultured cells using 300 μg total protein lysate from cells, 10 μl Protein G Sepharose (Amersham) and 5 μl AR-specific antibody (N-20). For experiments involving coprecipitation of AR, we lysed cells in molybdate-containing lysis buffer[11,12,16]. Immunoprecipitation from mouse tissues was performed using 1 mg total protein lysed in CelLytic-M (Sigma). R.S.I. was computed as the signal intensity of each sample divided by that of AR-24Q cells, DMSO-treated cells or DMSO-treated mice.

Pulse-chase labeling assay. We transfected cells as described above, starved them for 1 h, and then labeled them for 1 h with 150 μCi of Redivue Pro-Mix L-[35S] *in vitro* cell-labeling mix (Amersham) per milliliter. We chased the cells for the indicated time intervals in complete medium with DMSO or 360 nM 17-AAG. We performed immunoprecipitation using equivalent amounts of protein lysates as described above, and analyzed by phosphorimaging (Typhoon 8600 phosphorimager; Amersham) and Image Gauge software, version 4.22 (Fujifilm).

Quantitative real-time RT-PCR. We determined the levels of AR mRNA by real-time Taqman PCR by the iCycler system (Bio-Rad) as previously described[50]. R.S.I. was computed as the signal intensity of each sample divided by that of DMSO-treated cells or DMSO-treated control mice.

Immunohistochemistry and histopathology. We prepared tissues as previously described[35–38]. We incubated the tissue sections with expanded polyQ-specific antibody (1:10,000, 1C2; Chemicon) and GFAP-specific antibody (1:1,000, Boehringer Manheim). We air-dried 6 μm–thick paraffin-embedded sections of the gastrocnemius muscles and stained them with hematoxylin and eosin. For quantification of 1C2-positive cells, we counted the number of 1C2-positive cells of the thoracic spinal cord and gastrocnemius muscle in each individual mouse as previously described[36].

Statistical analysis. We analyzed data by unpaired *t*-tests and Kaplan-Meier and log-rank tests for survival rate using Statview software version 5 (HULINKS). We examined statistical significance of the drug-dose dependency by the Williams test for multiple comparisons using Microsoft Excel 2004 (Microsoft).

Accession codes. BIND identifiers (http://bind.ca): 316918.

Note: Supplementary information is available on the Nature Medicine website.

ACKNOWLEDGMENTS

We thank National Cancer Institute and Kosan Biosciences for kindly providing 17-AAG. This work was supported by a Center of Excellence (COE) grant from the Ministry of Education, Culture, Sports, Science and Technology, Japan, and by grants from the Ministry of Health, Labor and Welfare, Japan.

COMPETING INTERESTS STATEMENT

The authors declare that they have no competing financial interests.

Published online at http://www.nature.com/naturemedicine/
Reprints and permissions information is available online at http://npg.nature.com/reprintsandpermissions/

1. Pratt, W.B. & Toft, D.O. Regulation of signaling protein function and trafficking by the hsp90/hsp70-based chaperone machinery. *Exp. Biol. Med. (Maywood)* **228**, 111–133 (2003).
2. Neckers, L., Schulte, T.W. & Mimnaugh, E. Geldanamycin as a potential anti-cancer agent: its molecular target and biochemical activity. *Invest. New Drugs* **17**, 361–373 (1999).
3. Supko, J.G., Hickman, R.L., Grever, M.R. & Malspeis, L. Preclinical pharmacologic evaluation of geldanamycin as an antitumor agent. *Cancer Chemother. Pharmacol.* **36**, 305–315 (1995).
4. Schulte, T.W. & Neckers, L.M. The benzoquinone ansamycin 17-allylamino-17-demethoxygeldanamycin binds to HSP90 and shares important biologic activities with geldanamycin. *Cancer Chemother. Pharmacol.* **42**, 273–279 (1998).
5. Page, J. *et al.* Comparison of geldanamycin (NSC-122750) and 17-allylaminogeldanamycin (NSC-330507D) toxicity in rats. *Proc. Am. Assoc. Cancer Res.* **38**, 308 (1997).
6. Sullivan, W. *et al.* Nucleotides and two functional states of hsp90. *J. Biol. Chem.* **272**, 8007–8012 (1997).
7. Bagatell, R. *et al.* Destabilization of steroid receptors by heat shock protein 90-binding drugs: a ligand-independent approach to hormonal therapy of breast cancer. *Clin. Cancer Res.* **7**, 2076–2084 (2001).
8. Neckers, L. Heat shock protein 90 inhibition by 17-allylamino-17-demethoxygeldanamycin: a novel therapeutic approach for treating hormone-refractory prostate cancer. *Clin. Cancer Res.* **8**, 962–966 (2002).
9. Felts, S.J. & Toft, D.O. p23, a simple protein with complex activities. *Cell Stress Chaperones* **8**, 108–113 (2003).
10. Johnson, J.L. & Toft, D.O. Binding of p23 and hsp90 during assembly with the progesterone receptor. *Mol. Endocrinol.* **9**, 670–678 (1995).
11. Smith, D.F. *et al.* Progesterone receptor structure and function altered by geldanamycin, an hsp90-binding agent. *Mol. Cell. Biol.* **15**, 6804–6812 (1995).
12. Whitesell, L. & Cook, P. Stable and specific binding of heat shock protein 90 by geldanamycin disrupts glucocorticoid receptor function in intact cells. *Mol. Endocrinol.* **10**, 705–712 (1996).
13. Schneider, C. *et al.* Pharmacologic shifting of a balance between protein refolding and degradation mediated by Hsp90. *Proc. Natl. Acad. Sci. USA* **93**, 14536–14541 (1996).
14. Solit, D.B. *et al.* 17-Allylamino-17-demethoxygeldanamycin induces the degradation of androgen receptor and HER-2/neu and inhibits the growth of prostate cancer xenografts. *Clin. Cancer Res.* **8**, 986–993 (2002).
15. Vanaja, D.K., Mitchell, S.H., Toft, D.O. & Young, C.Y. Effect of geldanamycin on androgen receptor function and stability. *Cell Stress Chaperones* **7**, 55–64 (2002).
16. Beliakoff, J. *et al.* Hormone-refractory breast cancer remains sensitive to the antitumor activity of heat shock protein 90 inhibitors. *Clin. Cancer Res.* **9**, 4961–4971 (2003).
17. Bonvini, P., Dalla Rosa, H., Vignes, N. & Rosolen, A. Ubiquitination and proteasomal degradation of nucleophosmin-anaplastic lymphoma kinase induced by 17-allylamino-demethoxygeldanamycin: role of the co-chaperone carboxyl heat shock protein 70-interacting protein. *Cancer Res.* **64**, 3256–3264 (2004).
18. Mimnaugh, E.G., Chavany, C. & Neckers, L. Polyubiquitination and proteasomal degradation of the p185c-erbB-2 receptor protein-tyrosine kinase induced by geldanamycin. *J. Biol. Chem.* **271**, 22796–22801 (1996).
19. Kamal, A. *et al.* A high-affinity conformation of Hsp90 confers tumour selectivity on Hsp90 inhibitors. *Nature* **425**, 407–410 (2003).
20. Whitesell, L., Bagatell, R. & Falsey, R. The stress response: implications for the clinical development of hsp90 inhibitors. *Curr. Cancer Drug Targets* **3**, 349–358 (2003).
21. Muchowski, P.J. & Wacker, J.L. Modulation of neurodegeneration by molecular chaperones. *Nat. Rev. Neurosci.* **6**, 11–22 (2005).
22. Sittler, A. *et al.* Geldanamycin activates a heat shock response and inhibits huntingtin aggregation in a cell culture model of Huntington's disease. *Hum. Mol. Genet.* **10**, 1307–1315 (2001).
23. Hay, D.G. *et al.* Progressive decrease in chaperone protein levels in a mouse model of Huntington's disease and induction of stress proteins as a therapeutic approach. *Hum. Mol. Genet.* **13**, 1389–1405 (2004).
24. Auluck, P.K. & Bonini, N.M. Pharmacological prevention of Parkinson disease in *Drosophila*. *Nat. Med.* **8**, 1185–1186 (2002).
25. Dou, F. *et al.* Chaperones increase association of tau protein with microtubules. *Proc. Natl. Acad. Sci. USA* **100**, 721–726 (2003).

26. Petrucelli, L. *et al.* CHIP and Hsp70 regulate tau ubiquitination, degradation and aggregation. *Hum. Mol. Genet.* **13**, 703–714 (2004).
27. Lui, A., Ran, R., Parmentier-Batteur, S., Nee, A. & Sharp, F.R. Geldanamycin induces heat shock proteins in brain and protects against focal cerebral ischemia. *J. Neurochem.* **81**, 355–364 (2002).
28. Murphy, P. *et al.* Suppressive effects of ansamycins on inducible nitric oxide synthase expression and the development of experimental autoimmune encephalomyelitis. *J. Neurosci. Res.* **67**, 461–470 (2002).
29. La Spada, A.R., Wilson, E.M., Lubahn, D.B., Harding, A.E. & Fischbeck, K.H. Androgen receptor gene mutations in X-linked spinal and bulbar muscular atrophy. *Nature* **352**, 77–79 (1991).
30. Sabue, G. *et al.* X-linked recessive bulbospinal neuronopathy. A clinicopathological study. *Brain* **112**, 209–232 (1989).
31. Zoghbi, H.Y. & Orr, H.T. Glutamine repeats and neurodegeneration. *Annu. Rev. Neurosci.* **23**, 217–247 (2000).
32. Tanaka, F. *et al.* Founder effect in spinal and bulbar muscular atrophy (SBMA). *Hum. Mol. Genet.* **5**, 1253–1257 (1996).
33. Doyu, M. *et al.* Severity of X-linked recessive bulbospinal neuronopathy correlates with size of the tandem CAG repeat in androgen receptor gene. *Ann. Neurol.* **32**, 707–710 (1992).
34. Adachi, H. *et al.* Widespread nuclear and cytoplasmic accumulation of mutant androgen receptor in SBMA patients. *Brain* **128**, 659–670 (2005).
35. Katsuno, M. *et al.* Testosterone reduction prevents phenotypic expression in a transgenic mouse model of spinal and bulbar muscular atrophy. *Neuron* **35**, 843–854 (2002).
36. Adachi, H. *et al.* Heat shock protein 70 chaperone overexpression ameliorates phenotypes of the spinal and bulbar muscular atrophy transgenic mouse model by reducing nuclear-localized mutant androgen receptor protein. *J. Neurosci.* **23**, 2203–2211 (2003).
37. Katsuno, M. *et al.* Leuprorelin rescues polyglutamine-dependent phenotypes in a transgenic mouse model of spinal and bulbar muscular atrophy. *Nat. Med.* **9**, 768–773 (2003).
38. Minamiyama, M. *et al.* Sodium butyrate ameliorates phenotypic expression in a transgenic mouse model of spinal and bulbar muscular atrophy. *Hum. Mol. Genet.* **13**, 1183–1192 (2004).
39. Bailey, C.K., Andriola, I.F., Kampinga, H.H. & Merry, D.E. Molecular chaperones enhance the degradation of expanded polyglutamine repeat androgen receptor in a cellular model of spinal and bulbar muscular atrophy. *Hum. Mol. Genet.* **11**, 515–523 (2002).
40. Lieberman, A.P., Harmison, G., Strand, A.D., Olson, J.M. & Fischbeck, K.H. Altered transcriptional regulation in cells expressing the expanded polyglutamine androgen receptor. *Hum. Mol. Genet.* **11**, 1967–1976 (2002).
41. Zou, J., Guo, Y., Guettouche, T., Smith, D.F. & Voellmy, R. Repression of heat shock transcription factor HSF1 activation by HSP90 (HSP90 complex) that forms a stress-sensitive complex with HSF1. *Cell* **94**, 471–480 (1998).
42. Egorin, M.J. *et al.* Plasma pharmacokinetics and tissue distribution of 17-(allylamino)-17-demethoxygeldanamycin (NSC 330507) in CD2F1 mice1. *Cancer Chemother. Pharmacol.* **47**, 291–302 (2001).
43. Ravikumar, B. *et al.* Inhibition of mTOR induces autophagy and reduces toxicity of polyglutamine expansions in fly and mouse models of Huntington disease. *Nat. Genet.* **36**, 585–595 (2004).
44. Ferrante, R.J. *et al.* Chemotherapy for the brain: the antitumor antibiotic mithramycin prolongs survival in a mouse model of Huntington's disease. *J. Neurosci.* **24**, 10335–10342 (2004).
45. Cummings, C.J. *et al.* Chaperone suppression of aggregation and altered subcellular proteasome localization imply protein misfolding in SCA1. *Nat. Genet.* **19**, 148–154 (1998).
46. Kobayashi, Y. *et al.* Chaperones Hsp70 and Hsp40 suppress aggregate formation and apoptosis in cultured neuronal cells expressing truncated androgen receptor protein with expanded polyglutamine tract. *J. Biol. Chem.* **275**, 8772–8778 (2000).
47. Blagosklonny, M.V., Toretsky, J., Bohen, S. & Neckers, L. Mutant conformation of p53 translated *in vitro* or *in vivo* requires functional HSP90. *Proc. Natl. Acad. Sci. USA* **93**, 8379–8383 (1996).
48. Yamamoto, A., Lucas, J.J. & Hen, R. Reversal of neuropathology and motor dysfunction in a conditional model of Huntington's disease. *Cell* **101**, 57–66 (2000).
49. Xia, H. *et al.* RNAi suppresses polyglutamine-induced neurodegeneration in a model of spinocerebellar ataxia. *Nat. Med.* **10**, 816–820 (2004).
50. Ishigaki, S. *et al.* X-Linked inhibitor of apoptosis protein is involved in mutant SOD1-mediated neuronal degeneration. *J. Neurochem.* **82**, 576–584 (2002).

Gene Expression Profile of Spinal Motor Neurons in Sporadic Amyotrophic Lateral Sclerosis

Yue-Mei Jiang, PhD,[1] Masahiko Yamamoto, MD,[1] Yasushi Kobayashi, MD,[1] Tsuyoshi Yoshihara, PhD,[1] Yideng Liang, PhD,[1] Shinichi Terao, MD,[2] Hideyuki Takeuchi, MD,[1] Shinsuke Ishigaki, MD,[1] Masahisa Katsuno, MD,[1] Hiroaki Adachi, MD,[1] Jun-ichi Niwa, MD,[1] Fumiaki Tanaka, MD,[1] Manabu Doyu, MD,[1] Mari Yoshida, MD,[3] Yoshio Hashizume, MD,[3] and Gen Sobue, MD[1]

The causative pathomechanism of sporadic amyotrophic lateral sclerosis (ALS) is not clearly understood. Using microarray technology combined with laser-captured microdissection, gene expression profiles of degenerating spinal motor neurons isolated from autopsied patients with sporadic ALS were examined. Gene expression was quantitatively assessed by real-time reverse transcription polymerase chain reaction and in situ hybridization. Spinal motor neurons showed a distinct gene expression profile from the whole spinal ventral horn. Three percent of genes examined were downregulated, and 1% were upregulated in motor neurons. Downregulated genes included those associated with cytoskeleton/axonal transport, transcription, and cell surface antigens/receptors, such as dynactin, microtubule-associated proteins, and early growth response 3 (EGR3). In contrast, cell death–associated genes were mostly upregulated. Promoters for cell death pathway, death receptor 5, cyclins A1 and C, and caspases-1, -3, and -9, were upregulated, whereas cell death inhibitors, acetyl-CoA transporter, and NF-κB were also upregulated. Moreover, neuroprotective neurotrophic factors such as ciliary neurotrophic factor (CNTF), Hepatocyte growth factor (HGF), and glial cell line–derived neurotrophic factor were upregulated. Inflammation-related genes, such as those belonging to the cytokine family, were not, however, significantly upregulated in either motor neurons or ventral horns. The motor neuron–specific gene expression profile in sporadic ALS can provide direct information on the genes leading to neurodegeneration and neuronal death and are helpful for developing new therapeutic strategies.

Ann Neurol 2005;57:236–251

Amyotrophic lateral sclerosis (ALS) is a devastating neurodegenerative disease characterized by loss of motor neurons in the spinal cord, brainstem, and motor cortex.[1] Initial symptoms include weakness of the limbs, abnormalities of speech, and difficulties in swallowing. The weakness ultimately progresses to complete paralysis, and half of the patients die within 3 years after the onset of symptoms, mostly because of respiratory failure. Approximately 10% of all ALS patients show familial traits, and 20 to 30% of familial ALS patients are associated with a mutation in the copper/zinc superoxide dismutase 1 gene (SOD1). However, more than 90% of ALS patients are sporadic, not showing any familial trait. The presence of Bunina bodies in the remaining spinal motor neurons is a hallmark of sporadic ALS cases.[2,3] So far, several hypotheses about the pathogenesis of sporadic ALS have been proposed based on extensive research on sporadic ALS: oxidative stress, glutamate excitotoxicity, impaired axonal transport, mitochondrial dysfunction, neurotrophic deprivation, proteasomal dysfunction, neuroinflammation, autoimmunity, viral infection, and others.[4–11] Nevertheless, the actual pathogenic mechanism of the selective motor neuron degeneration and ultimate cell death in sporadic ALS remains unknown. There have been extensive studies using animal models and culture systems for familial ALS, especially with SOD1 mutations, but no similar approach is available for studying sporadic ALS.

Recently advances in DNA microarray technology make it possible to analyze global gene expression profiles of thousands of genes in normal as well as pathological tissues. Global gene expression studies using DNA microarray technology have generated valuable

From the [1]Department of Neurology, Nagoya University Graduate School of Medicine, Nagoya; [2]Department of Internal Medicine, Aichi Medical University School of Medicine; and [3]Department of Neuropathology, Institute for Medical Science of Aging, Aichi Medical University School of Medicine, Nagakute, Aichi, Japan.

Received Sep 7, 2004, and in revised form Oct 22. Accepted for publication Nov 14, 2004.

Published online Jan 26, 2005, in Wiley InterScience (www.interscience.wiley.com). DOI: 10.1002/ana.20379

Address correspondence to Dr Sobue, Department of Neurology, Nagoya University Graduate School of Medicine, Nagoya 466-8550, Japan. E-mail: sobueg@med.nagoya-u.ac.jp

information about cell behavior in tissues consisting of homogeneous cell types, cultured cells, and cancer tissues of monoclonal origin.[12,13] In the case of neuronal tissues, particularly those of patients with neurological diseases, however, the complexity of tissues containing multiple lineages of cells, such as neurons, glial cells, and vascular tissues, places limitations on the use of DNA microarray technology. In the lesions of ALS spinal cords, there are reduced numbers of motor neurons with glial cell proliferation, making it difficult to examine motor neuron–specific gene expression.

Laser-captured microdissection (LCM) has been reported to make it possible to isolate single individual neurons from neural tissues with well-preserved mRNA quality.[14,15] In addition, RNA amplification techniques preserving the relative amounts of individual mRNAs have been developed recently.[16,17] LCM and RNA amplification combined with DNA microarray analyses have been reported to enable studies of cell type–specific gene expression profiles in tissues with multiple cell lineages.[16,18] Such integrated analysis system provide an effective tool for investigating the cellular events affecting cell type–specific gene expression profiles in neurodegenerative diseases such as ALS. Indeed, we and other groups demonstrated that these integrated systems could be applied successfully to describe cell-specific gene expression profiles in neuronal tissues.[15,18]

In this study, we applied integrated LCM, RNA amplification, and DNA microarray analysis to clarify alterations of motor neuron–specific gene expression in sporadic ALS cases and successfully obtained expression gene database in situ from degenerating motor neurons in sporadic ALS spinal cord.

Patients and Methods

Tissues from Amyotrophic Lateral Sclerosis and Control Patients

Fresh specimens of lumbar spinal cord (L4 to L5 segment) from 14 sporadic ALS patients (nine men, five women) and 13 neurologically normal patients (nine men, four women) were obtained at autopsy (Table 1). Diagnosis of ALS was

Table 1. Details of Patients Examined in This Study

Patients	Sex	Age (yr)	Duration of Illness (yr)	Postmortem Delay (hr)	Diseases	Spinal Cord Neuropathology Motor Neuron Loss/Gliosis
ALS1	M	72	3.7	6	ALS (B, UL, LL)	Moderate/mild
ALS2	M	71	2.3	5	ALS (LL, UL)	Moderate/mild
ALS3	M	58	1.8	13	ALS (UL, LL, B)	Severe/severe
ALS4	M	43	2.6	5	ALS (LL, B)	Moderate/mild
ALS5	M	53	2.8	11	ALS (B, UL, LL)	Moderate/severe
ALS6	F	79	4.0	4	ALS (UL, LL, B)	Severe/severe
ALS7	F	59	2.5	3	ALS (UL)	Mild/mild
ALS8	F	67	2.0	7	ALS (UL, B)	Severe/mild
ALS9	M	74	4.3	10	ALS (LL, B)	Severe/mild
ALS10	F	47	1.8	4	ALS (B, UL, LL)	Mild/mild
ALS11	M	74	4.5	12	ALS (UL, LL)	Moderate/mild
ALS12	M	57	3.5	5	ALS (LL, UL)	Severe/mild
ALS13	F	53	3.0	8	ALS (B, UL, LL)	Severe/severe
ALS14	M	63	2.2	5	ALS (UL, B)	Mild/mild
Control1	M	57	—	7	Pneumonia	No
Control2	M	78	—	10	Cerebral infarction	No
Control3	M	72	—	9	Lung cancer	No
Control4	F	52	—	7	Pneumonia	No
Control5	F	65	—	12	Pneumonia	No
Control6	M	75	—	10	Heart failure	No
Control7	M	42	—	5	Heart failure	No
Control8	F	76	—	5	Pancreas cancer	No
Control9	F	84	—	6	Myocardial infarction	No
Control10	M	48	—	13	Heart failure	No
Control11	M	77	—	11	Heart failure	No
Control12	M	66	—	11	Cerebral infarction	No
Control13	M	75	—	4	Pneumonia	No

The age, duration of illness, and postmortem delay are indicated for the ALS and control cases. Predominant clinical features of ALS are shown: UL = upper limbs; LL = lower limbs; B = bulbar. Neuropathological involvement of spinal cords was graded as previously. Ten ALS samples were used for microarray analysis: five of them (1, 7, 10, 11, and 14) were analyzed using 4.8K array for spinal motor neurons; five (2, 4, 5, 8, and 12) using 1.0K for spinal motor neurons; five (1, 3, 10, 13, and 14) using 4.8K for spinal ventral horn gray matter; and five (1, 2, 4, 5, and 13) and five (1, 2, 7, 8, and 10) control samples using 4.8K and 1.0K. Thirteen ALS (1–13) and 11 (1–11) control samples were used for TaqMan reverse transcription polymerase chain reaction analysis. Five ALS (1, 10, 11, 13, and 14) and four control (1, 3, 5, and 12) samples were used for in situ hybridization and immunohistochemistry.
ALS = amyotrophic lateral sclerosis.

confirmed by El Escorial diagnostic criteria defined by the World Federation of Neurology and the histopathological findings, particularly the presence of the Bunina body.[2,3] All cases of ALS were sporadic and did not show any heredity. ALS patients with *SOD1* mutation were excluded. The collection of tissues and their use for this study were approved by the ethics committee of Nagoya University Graduate School of Medicine. Tissues were frozen immediately and stored at −80°C until use. The mean ages and standard deviations for ALS and control patients were 62.1 ± 11.0 and 66.7 ± 13.1 years, and the mean postmortem intervals and standard deviations were 7.0 ± 3.3 and 8.5 ± 3.0 hours, respectively. The differences between the means of either age or postmortem interval were not significant between the ALS and control groups. The cause of death in all ALS patients was respiratory failure, and the causes in the control patients were pneumonia, lung cancer, or acute heart failure (see Table 1). Parts of the lumbar spinal cord were fixed in 10% buffered formalin solution, and processed for paraffin sections. The sections were stained with hematoxylin and eosin and Klüver-Barrera and Holzer techniques, and histological assessment was performed. The degree of motor neuron loss and astrogliosis was ranked as mild, moderate or severe according to previously reported.[19,20]

Laser-Captured Microdissection of Spinal Motor Neurons

Sections (10μm) were cut with a standard cryostat, mounted on poly-L-lysin coated slides (Zeiss, Thornwood, NY), and stained with hematoxylin to identify the motor neurons located in the medial and lateral nuclei of the ventral horns of lumber spinal cords. After staining with hematoxylin, the sections were washed in RNase-free water and dried.[21,22] The PALM Robot-Microbeam system (P.A.L.M. Mikrolaser Technology AG, Bernried, Germany) was used for laser capture. The pulsed laser microbeam cut precisely around the targeted motor neurons in the spinal ventral horn (LCM; see Fig 1A–C). The identity of motor neurons was ascertained by reverse transcription polymerase chain reaction (RT-PCR) for choline acetyltransferase (ChAT) as described previously.[15] Each laser-isolated specimen subsequently was ejected from the glass slide with a single or several laser shots and collected directly into the cap of a PCR tube containing denaturing buffer by a process of laser pressure catapulting in the totally noncontact manner previously described.[23] The LCM-isolated cells (approximately 500 pooled cells) were dissolved in denaturing buffer (StrataPrep Total RNA Microprep Kit; Stratagene, San Diego, CA) and stored at −80°C until use.

RNA Extraction of Laser-Captured Microdissection Motor Neuron Samples and Spinal Ventral Horn Homogenates

LCM-isolated cells in denaturing buffer were thawed and centrifuged briefly before the RNA was extracted using a StrataPrep Total RNA Microprep Kit (Stratagene) according to the manufacturer's protocol. RNA was extracted as well from the total homogenates of ventral horn gray matter of spinal cords,[19] which was dissected under a dissecting microscope.

Reverse Transcription and T7 RNA Polymerase Amplification of RNA

Ten microliters of purified RNA obtained as described above was mixed with 1μl of 0.5μg/ml T7-oligodT primer (5′-TCTAGTCGACGGCCAGTGAATTGTAATACGACTCACTATAGGGCGT$_{21}$-3′) to initiate first-strand synthesis. The primer and RNA were incubated in 4μl of 5 × first-strand reaction buffer, 0.1M DTT (2μl), 10mM dNTPs (1μl), 1μl of RNasin, and 1μl of Superscript II reverse transcriptase (Invitrogen, Carlsbad, CA) at 42°C for 1 hour, and then 30μl of 5 × second-strand synthesis buffer, 10mM dNTPs (3μl), 4μl of DNA polymerase, 1μl of *Escherichia coli* RNase H, and 1μl of *E. coli* DNA ligase and 91μl of RNase-free H_2O were added, and the mixture was incubated at 16°C for 2 hours and then at 16°C for 10 minutes after the addition of 2μl of T4 DNA polymerase. Next, an Ampliscribe T7 Transcription Kit (Epicentre Technologies, Madison, WI) was used for RNA amplification: 8μl double-stranded cDNA, 2μl of 10 × Ampliscribe T7 buffer, 1.5μl each of 100mM ATP, CTP, GTP, and UTP, 0.1 M DTT (2μl), and 2μl of T7 RNA polymerase were incubated at 42°C for 3 hours.

For second-round amplification, 10μl of amplified RNA (aRNA) from first-round amplification was mixed together with 1μl of 1mg/ml random hexamers (Invitrogen), and then first-stranded cDNA was synthesized, followed by second-stranded cDNA synthesis as described above. The double-stranded cDNA was subjected to second-round T7 in vitro transcription as above and then subsequent third-round aRNA amplification. After third-round amplification, aRNA was treated with DNase (Wako, Kanagawa, Japan) and cleaned up using an RNeasy Kit (Qiagen, Valencia, CA) according to the manufacturer's protocol.

DNA Microarray Analysis

Fluorescent cDNA probes were synthesized from aRNA of laser-captured spinal motor neurons and RNA from ventral spinal tissue homogenates using an Atlas Glass Fluorescent Labeling Kit (Clontech, Palo Alto, CA) according to the manufacturer's protocol. Cy3-labeled cDNA probes were synthesized from ALS samples for spinal motor neurons and homogenates, and Cy5-labeled cDNA probes were synthesized from control samples. BD Atlas Glass Microarray Human 1.0 and 3.8 (Clontech) slides were hybridized with these fluorescent labeled probes overnight at 50°C and then washed four times and dried according to the manufacturer's protocol. Individual Cy3-labeled cDNA probes from ALS RNA samples of spinal motor neurons and homogenates for each patient were coupled with Cy5-labeled cDNA probes from control RNA samples of those tissues, which were prepared by mixing equal amounts of RNA samples amplified from the control patients. The microarrays were scanned in a laser scanner (GenePix 4000; Axon Instruments, Union City, CA), and the resulting signals were quantified and stored using GenePix Pro analysis software (Axon Instruments). The data for each expressed gene obtained from microarray analysis were expressed as the ratios of the values of individual ALS patients or the means of the values of ALS to the values of the control patients. The values of gene expression levels were means-calculated from motor neurons of 5 or 10 inde-

pendent individuals with ALS as well as from spinal ventral horns of 5 individuals with ALS.

Quantitative Real-Time Reverse Transcription Polymerase Chain Reaction

The probe and primers for the real-time PCR were designed using Primer3′ (S. Rozen and H. J. Skaletsky, available at http://www-genome.wi.mit.edu/genome_software/other/primer3.html). TaqMan PCR was conducted using an iCycler system (Bio-Rad Laboratories, Hercules, CA) with a QuantiTect Probe PCR Kit (Qiagen) and the cDNA according to the manufacturer's protocol. The reaction conditions were 95°C for 3 minutes and then 50 cycles of 15 seconds at 95°C followed by 60 seconds at 55°C. All experiments were performed in quadruplicate, and several negative controls were included. For an internal standard control, the expression of glyceraldehyde-3-phosphate dehydrogenase (GAPDH) was simultaneously quantified. The primers and probe sequences for the examined genes (acetyl-CoA transporter: D88152; Bak: NM_001188; CRABP1: NM_004378; cyclin C: M74091; dynactin 1: NM_004082; EGR3: NM_004430; ephrin A1: M57730; GAPDH: NM_002046; KIAA0231: D86984; and TrkC: U05012) were described in the legends for Figure 3. The threshold cycles of each gene were determined as the number of PCR cycles at which the increase in reporter fluorescence reached 10 times above the baseline signal. The weight ratio of the target gene to GAPDH gives the standardized expression level.

In Situ Hybridization

Frozen sections (10μm thick) of the spinal cord were prepared and immediately fixed in 4% paraformaldehyde. Then, they were treated with 0.1% diethylpyrocarbonate (DEPC) twice for 15 minutes and prehybridized at 45°C for 1 hour. Digoxigenin-labeled cRNA probes were generated from linearized plasmids for the genes of interest using SP6 or T7 polymerase (Roche Diagnostics, Basel, Switzerland). Gene names, Genebank accession number, probe position (nucleotide number), and probe size were as follows: acetyl-CoA transporter, D88152, nucleotides 397-741, 345bp; Bak, NM_001188, nucleotides 792–2094, 345bp; CRABP1, NM_004378, nucleotides 210–545, 336bp; dynactin 1, NM_004082, nucleotides 2392–2774, 383bp; DR5, NM_004082, nucleotides 682–1070, 389bp; EGR3, NM_004430, nucleotides 1433–1794, 362bp; KIAA0231, D86984, nucleotides 698–1053, 356bp; TrkC, U05012, nucleotides 1412–1721, 310bp. After prehybridization, the sections were hybridized with each digoxigenin-labeled cRNA probe overnight at 45°C. The washed sections were incubated with alkaline phosphatase-conjugated anti–digoxigenin antibody (Roche Diagnostics). The signal was visualized with NBT/BCIP (Roche Diagnostics).

Immunohistochemistry

Frozen sections (10μm thick) of the spinal cord were prepared and immediately fixed in 4% paraformaldehyde. Then, they were blocked with 2% bovine serum albumin (Sigma) in Tris-buffered saline at room temperature for 20 minutes and incubated with anti–cyclin C (1:200 dilution; Santa Cruz Biotechnology, Santa Cruz, CA) antibody overnight at 4°C. Subsequent procedures were performed using ENVISION++KIT/HRP (diaminobenzidine tetrahydrochloride; DAKO, Carpinteria, CA) according to the manufacturer's protocol.

Statistical Analyses

To assess the correlation of intensity values for each labeling sample, we used scatterplots and measured linear relationships. The correlation coefficient, R^2, that was calculated indicates the variability of intensity values between Cy-5– and Cy-3–labeled samples. To perform cluster analyses of hierarchical clustering, self-organizing maps (SOM) and principal component analysis after logarithmic transformation, we used Acuity 3.0 software (Axon Instruments). The data measured by quantitative real-time RT-PCR analysis were analyzed by Student's t tests.

Results

T7 Amplification Preserves Gene Expression Profiles

Because the amounts of laser-microdissected samples were extremely low and did not contain enough mRNA for further analysis, RNA amplification was required. It was critical to achieve sufficient RNA amplification and yet maintain the expression profiles of mRNAs. We performed experiments to determine how the expression profiles of mRNAs were affected by the T7 amplification procedure. RNA samples were extracted from control spinal cords and a part of RNA samples was amplified using T7 amplification. One flourescently labeled probe was synthesized from an individually amplified RNA (aRNA) or nonamplified RNA (nRNA) and was hybridized to microarrays. Independent amplification of RNA yielded quite similar expression patterns. The correlation of signal intensities between independent amplifications for the third aRNA was $R^2 = 0.9157$, $p < 0.0001$, and on the other hand, the correlation of signal intensities in nRNA was $R^2 = 0.9157$, $p < 0.0001$ (Fig 1D, E). Previous reports using similar amplification procedures as ours also have confirmed the reproducibility of T7 amplification for the preservation of RNA expression profiles.[14,15,17] In this study, the third-round amplification was performed for the LCM-isolated motor neurons, but for the spinal ventral horn homogenates a single amplification produced enough RNA for further analysis, and similar expression patterns were found between the first and third amplifications (data not shown).

Gene Expression Database of Spinal Motor Neurons and Ventral Horn Homogenates of Amyotrophic Lateral Sclerosis

aRNA samples from the motor neurons and the ventral horn homogenates from the lumbar spinal cords were subjected to microarray analysis. The differences of the gene expression levels between ALS and control sam-

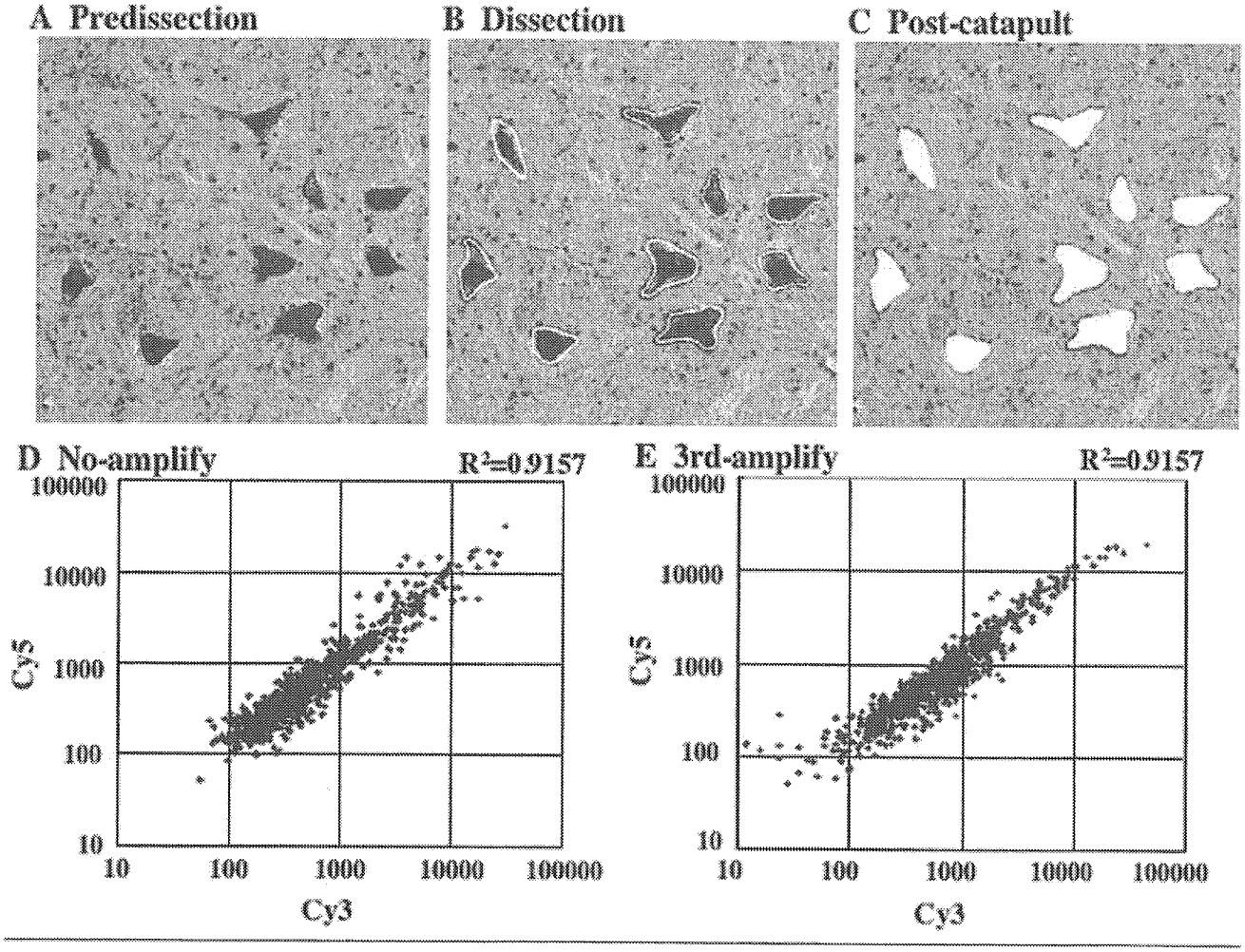

Fig 1. Verification of laser-captured microdissection (LCM) and RNA amplification. Microdissection of motor neurons in spinal ventral horn: sections were stained with hematoxylin (A); margins of motor neurons were dissected by the laser beam (B); and motor neurons were isolated from slides by laser pressure catapulting (C). Scatterplots of nonamplified and amplified RNAs: correlations between independent amplifications of control spinal cord samples are shown using nonamplified (D) and third amplified RNAs (E). These RNAs were split into two samples for labeling of Cy5 and Cy3 and hybridized separately to two microarrays. The very high squared correlations reflect the high reproducibility of the hybridization results with the same values between nonamplified and third amplified RNAs.

ples were expressed as ratios of the values of ALS individuals compared with the mean values of the controls. One percent (52/4,845) of genes examined were significantly upregulated in spinal motor neurons of ALS patients and 3% (144/4,845) were downregulated, assuming that the changes of 3.0-fold increase and 0.3-fold decrease were significant, when the mean levels of gene expression were calculated. In contrast with motor neurons, the total spinal ventral horn homogenates demonstrated 0.7% (37/4,845) and 0.2% (8/4,845) significant upregulation and downregulation of gene expression, respectively.

The genes prominently altered in ALS are listed in Tables 2 to 5 for spinal motor neurons and spinal ventral horn homogenates, respectively. Several upregulated genes listed were overlapping between spinal motor neurons (see Table 2) and ventral horns (see Table 4), suggesting that motor neuron overexpression is reflected to some extent by gene expression in ventral horn homogenates. The other genes upregulated in motor neurons were not present in the list for spinal ventral horns, because these gene expression changes were diluted and masked by changes occurring in other cell types. Because the number of spinal motor neurons was decreased in ALS spinal cords, most genes that were listed as downregulated genes in motor neurons (see Table 3) were not found in spinal ventral horns (see Table 5) except for three genes (CRABP1, EGR3, and postmeiotic segregation increased 2-like 11). When we categorized these altered genes in ALS motor neurons into several functional groups, the genes related to cell receptors and intracellular signaling, transcription,

Table 2. Upregulated Genes in ALS Motor Neurons (Top 30)

GeneBank No.	Gene Name	Fold Change (ALS/control)
NM_003419	Zinc finger protein 10 (KOX 1)	8.86
U91618	Neurotensin/neuromedin N precursor	8.33*
NM_004651	Ubiquitin-specific protease 11	8.13
D86984	KIAA0231	7.31*
A26792	Ciliary neuronotrophic factor (CNTF)	6.76
M77830	Desmoplakin I & II (DSP; DPI & DPII)	6.10
NM_005622	SA (rat hypertension-associated) homolog	5.47
NM_004733	Acetyl-coenzyme A transporter	5.33
NM_000021	Presenilin 1 (Alzheimer disease 3)	4.96
K03020	Phenylalanine-4-hydroxylase (PAH)	4.95*
AF016268	Death receptor 5 (DR5); cytotoxic TRAIL receptor, TNFR10b	4.91*
M74091	G1/S-specific cyclin C (CCNC)	4.82*
NM_000275	Oculocutaneous albinism II	4.78
AF000936	SH3-binding protein 2	4.73*
NM_000384	Apolipoprotein B	4.70
M63099	Interleukin-1 receptor antagonist	4.66*
M57730	Ephrin-A1	4.57*
L19067	NF-κ B transcription factor p65 subunit	4.52*
U66838	Cyclin A1 (CCNA1)	4.51*
NM_005021	Ectonucleotide pyrophosphatase/phosphodiesterase 3	4.48
NM_001550	Interferon-related developmental regulator 1	4.45
L25851	Integrin alpha E precursor (ITGAE)	4.43*
X16416	C-abl1 protooncogene	4.41
U08015	Transcription factor NF-ATc	4.40*
U44378	Mothers against dpp homolog 4 (SMAD4)	4.35*
NM_005067	Seven in absentia (Drosophila) homolog 2	4.22
J04536	Leukosialin precursor; sialophorin	4.19*
X06745	DNA polymerase alpha catalytic subunit	4.15*
U09564	Serine kinase	4.09*
U37139	β 3-endonexin	4.06*

Gene expression levels are expressed as means of fold-change, which is calculated by dividing the signals of each ALS sample by those of control samples, in the 5 or 10 (denoted by asterisk) patients with ALS.
ALS = amyotrophic lateral sclerosis.

metabolism, and cytoskeletal architecture were downregulated. The functional categories of secreted and extracellular communication proteins and cell cycle regulators were characteristically upregulated. A complete list of the differentially expressed genes is available online at http://www.med.nagoya-u.ac.jp/neurology/index.html.

Differential Gene Expression Profiles between Spinal Motor Neurons and Ventral Horn Homogenates of Amyotrophic Lateral Sclerosis

To compare the expression profile of motor neurons with that of spinal ventral horn homogenates, we performed cluster analyses. Because the patterns of gene expression from microarray analysis are impossible to discern by eye, data analysis software (Acuity 3.0 software; Axon Instruments) was used based on the dimensionality of the data: hierarchical clustering for high dimensional gene space and principal component analysis and SOM for low one. Hierarchical clustering clearly discriminated the expression profile of isolated motor neurons from that of ventral horn homogenates, showing two grouped branches of the dendrogram with a correlation coefficient of 0.446 (Fig 2A). Moreover, a principal component analysis confirmed the distinction of gene expression profiles between spinal motor neurons and ventral horns (see Fig 2B). The gene expression profile of motor neurons was clustered into a single cluster by the two clustering algorithms, which was well separated from that of spinal ventral horn gray matter, suggesting a relatively uniform degenerating process in spinal motor neurons in ALS.

Motor Neuron–Specific Gene Expression Profiles Identified by the Self-Organizing Map Analysis

To further analyze the expression pattern specific to spinal motor neurons, a SOM was produced as a nonhierarchical clustering.[24,25] The examined genes were subdivided into 25 clustered categories, and the selected genes are shown in a certain group of the SOM (see Fig 2C, Table 6). The genes contained in the clusters reflect the expression pattern in spinal motor neurons as well as that in spinal ventral horns, and these selected genes are somehow different from those in Tables 2 to 5 because of the different bases of classification. Clustering of the SOM showed motor neu-

Table 3. Downregulated Genes in ALS Motor Neurons (Bottom 30)

GeneBank No.	Gene Name	Fold Change (ALS/control)
NM_004378	Cellular retinoic acid–binding protein 1 (CRABP1)	0.12
NM_004430	Early growth response 3 (EGR3)	0.14
NM_005558	Ladinin 1	0.15
NM_003603	Arg/Abl-interacting protein ArgBP2	0.15
NM_000117	Emerin (Emery-Dreifuss muscular dystrophy)	0.15
NM_004357	CD151 antigen	0.15
X06820	Ras homolog gene family member B (RHOB)	0.15*
NM_003834	Regulator of G-protein signalling 11	0.16
NM_002960	S100 calcium-binding protein A3	0.16
NM_006289	Talin	0.16
NM_000964	Retinoic acid receptor, α	0.17
NM_002391	Midkine	0.17
M96944	Paired box protein PAX-5	0.17*
M74178	Hepatocyte growth factor–like protein	0.17*
NM_003822	Nuclear receptor subfamily 5, group A, member 2	0.17
NM_001188	BCL2-antagonist/killer 1; Bak	0.18
NM_000733	CD3E antigen, epsilon polypeptide (TiT3 complex)	0.18
NM_000408	Glycerol-3-phosphate dehydrogenase 2 (mitochondrial)	0.18
NM_000156	Guanidinoacetate *N*-methyltransferase	0.18*
M11886	Major histocompatibility complex, class I, C	0.18*
NM_003865	Homeo box (expressed in ES cells) 1	0.18
M36340	ADP-ribosylation factor 1 (ARF1)	0.18*
NM_001725	Bactericidal/permeability-increasing protein	0.18
NM_005334	Host cell factor C1 (VP16-accessory protein)	0.19
NM_004192	Acetylserotonin *O*-methyltransferase–like	0.19
NM_002684	Postmeiotic segregation increased 2–like 11	0.19
M11233	cathepsin D precursor (CTSD)	0.19*
NM_002313	Actin binding LIM protein 1	0.19
NM_002196	Insulinoma-associated 1	0.19
NM_002277	Keratin, hair, acidic, 1	0.19

Gene expression levels are expressed as means of fold-change, which is calculated by dividing the signals of each ALS sample by those of control samples, in the 5 or 10 (denoted by asterisk) patients with ALS.
ALS = amyotrophic lateral sclerosis.

ron–specific upregulated and downregulated gene expression commonly observed in five patients.

Clusters 1 (SOM1) and 6 (SOM6) contains 110 and 169 genes, respectively, that generally are downregulated in spinal motor neurons in all five cases examined, and those are known to be involved in the functional category of cell surface antigens and cell receptors, transcription, and cytoskeleton, whereas clusters 24 (SOM24) and 25 (SOM25) have 191 and 93 genes, respectively, that are predominantly upregulated in spinal motor neurons in all cases and belong to the functional category of cell signaling with extracellular communication, and cell death–associated proteins. The pattern of subcellular localization of their gene products also confirms the characteristics of the functional categories of upregulated and downregulated genes, that is, that plasma membrane and cytoskeletal proteins are more downregulated, and extracellular secreted proteins are more upregulated, in ALS motor neurons. All the genes listed in Table 3 are included in SOM1 and SOM6, whereas SOM24 and SOM25 do not contain all of the genes listed in Table 2. The former group of genes, with downregulation in motor neurons, included BCL2-antagonist/killer 1 (Bak) and TrkC receptor. Regarding genes related to transcription, early growth response 3 (EGR3), cellular retinoic acid–binding protein 1 (CRABP1), retinoic acid receptors, and Musashi 1 were included in SOM1 and SOM6 as downregulated genes. The expression of dynactin and microtubule-associated proteins (MAPs), which belong to the functional category of cytoskeleton and axonal transport, was downregulated in ALS motor neurons. On the other hand, KIAA0231 and acetyl-coenzyme A transporter were classified into the upregulated genes in motor neurons of ALS. Regarding genes related to cell death, the expression of cyclins A1 and C, death receptor 5 (DR5), and interleukin-1 receptor antagonist was upregulated together with that of NF-κB, tumor necrosis factor (TNF) receptor–associated factor 6 (TRAF6), and caspase-1, -3, and -9 in SOM24 and SOM25. For genes in the category of trophic factor cell signaling with extracellular communication, CNTF, HGF, and glial cell line–derived neurotrophic factor (GDNF) were upregulated in ALS motor neurons, whereas midkine was downregulated. The expression of vascular endothelial growth factor as

Table 4. Upregulated Genes in Spinal Ventral Horns of ALS (Top 30)

GeneBank	Gene Name	Fold Change (ALS/control)
NM_000508	Fibrinogen, A α polypeptide	8.23
D86984	KIAA0231	6.09
NM_001801	Cysteine dioxygenase, type I	5.81
X02544	α-1-Acid glycoprotein 1 precursor	5.59
NM_001973	ELK4, ETS-domain protein (SRF accessory protein 1)	5.12
NM_000021	Presenilin 1 (Alzheimer disease 3)	5.00
NM_002097	General transcription factor IIIA	4.96
U08015	Transcription factor NF-ATc	4.96
M57730	Ephrin-A1	4.88
U91618	Neurotensin/neuromedin N precursor	4.79
AF000936	SH3-binding protein 2	4.50
NM_002949	Mitochondrial ribosomal protein L12	4.11
NM_002386	Melanocortin 1 receptor	4.03
NM_001991	Enhancer of zeste (Drosophila) homolog 1	3.93
NM_000947	Primase, polypeptide 2A (58kDa)	3.92
NM_000239	Lysozyme (renal amyloidosis)	3.88
NM_001550	Interferon-related developmental regulator 1	3.67
NM_004602	Staufen (Drosophila, RNA-binding protein)	3.66
NM_000063	Complement component 2	3.58
NM_004651	Ubiquitin-specific protease 11	3.54
NM_000397	Cytochrome b-245, β polypeptide	3.51
NM_002056	Glutamine-fructose-6-phosphate transaminase 1	3.41
L25851	Integrin α E precursor (ITGAE)	3.36
NM_004616	Transmembrane 4 superfamily member 3	3.21
NM_003720	Down syndrome critical region gene 2	3.18
J04536	leukosialin precursor; sialophorin	3.15
X06745	DNA polymerase alpha catalytic subunit	3.15
K03020	Phenylalanine-4-hydroxylase (PAH)	3.14
NM_001329	C-terminal binding protein 2	3.14
NM_000276	Oculocerebrorenal syndrome of Lowe	3.13

Gene expression levels are expressed as means of fold-change, which is calculated by dividing the signals of each ALS sample by those of control samples, in the five patients with ALS.
ALS = amyotrophic lateral sclerosis.

well as NT-3 was unchanged. Furthermore, the genes whose expression was altered significantly in spinal ventral horn homogenates as shown in Tables 4 and 5 showed similar alterations to some extent in the remaining motor neurons. However, the upregulated genes, such as integrin αE and sialophorin for cell adhesion, which were demonstrated to be spinal ventral horn–derived (see Table 4) as well as spinal motor neuron–derived (Table 2) genes, were not sorted out into SOM24 and SOM25, indicating that their upregulation occurred predominantly in glial cells.

Data Confirmation with Quantitative Real-Time Reverse Transcription Polymerase Chain Reaction, In Situ Hybridization, and Immunohistochemistry

To assure the validity of the gene expression levels detected by microarray analysis, we performed quantitative real-time RT-PCR analysis on some genes of interest using a TaqMan PCR system. Because LCM-isolated motor neurons did not contain enough RNA to perform real-time RT-PCR analysis, only selected genes were assessed in motor neurons, and for other genes the spinal ventral horn homogenates were used as the template for quantitative RT-PCR. When the extent of increase or decrease of gene expression levels was expressed as the ratio of the genes of interest to GAPDH, acetyl-CoA transporter and KIAA0231 were significantly increased 3.1-fold ($p < 0.001$) and 3.3-fold ($p < 0.01$) in spinal motor neurons of ALS, respectively (Fig 3). EGR3 expression decreased to 0.27-fold ($p < 0.01$) in ALS motor neurons. These mRNA alterations were also detected at comparable levels when using spinal ventral horn homogenates of ALS (acetyl-CoA transporter, 1.8-fold increase [$p < 0.005$]; KIAA0231, 2.3-fold increase [$p < 0.05$]; and EGR3, 0.41-fold decrease [$p < 0.01$]). In addition, the gene expression of Bak and TrkC was downregulated 0.53-fold ($p < 0.01$) and 0.40-fold ($p < 0.05$) in ALS, respectively. Moreover, increases of ephrin A1 and cyclin C expression were observed to the extents of 2.5-fold ($p < 0.05$) and 4.9-fold ($p < 0.01$), whereas dynactin 1 mRNA was downregulated 0.44-fold ($p < 0.01$), and CRABP1 mRNA was also downregulated to 0.59-fold ($p < 0.01$) in ALS.

To further verify the localization and extent of expression of genes of interest, we performed in situ hy-

Table 5. Downregulated Genes in Spinal Ventral Horns of ALS (Bottom 30)

GeneBank	Gene Name	Fold Change (ALS/control)
NM_000843	Glutamate receptor, metabotropic 6	0.22
NM_000730	cholecystokinin A receptor	0.24
NM_003134	Signal recognition particle 14kDa	0.26
NM_003163	Syntaxin 1B	0.27
NM_006476	ATP synthase, H+ transporting, mitochondrial F1F0, subunit g	0.27
NM_001610	Acid phosphatase 2, lysosomal	0.28
NM_003108	SRY (sex determining region Y)-box 11	0.29
NM_001446	Fatty acid binding protein 7, brain	0.30
NM_004583	RAB5C, member RAS oncogene family	0.31
NM_001125	ADP-ribosylarginine hydrolase	0.31
NM_003320	Tubby (mouse) homolog	0.31
NM_001731	B-cell translocation gene 1, antiproliferative	0.31
NM_000999	Ribosomal protein L38	0.32
NM_004128	General transcription factor IIF, polypeptide 2 (30kDa subunit)	0.32
NM_001765	CD1C antigen, c polypeptide	0.32
NM_004430	Early growth response 3 (EGR3)	0.33
K00558	Tubulin, α, ubiquitous	0.33
NM_006732	FBJ murine osteosarcoma viral oncogene homolog B	0.33
NM_002040	GA-binding protein transcription factor, α subunit (60kDa)	0.34
NM_006161	Neurogenin 1	0.35
NM_002684	Postmeiotic segregation increased 2–like 11	0.35
NM_000801	FK506-binding protein 1A (12kDa)	0.35
NM_001051	Somatostatin receptor 3	0.35
NM_005017	Phosphate cytidylyltransferase 1, choline, alpha isoform	0.36
NM_004927	Chromosome 11 open reading frame 4	0.36
NM_000046	Arylsulfatase B	0.37
NM_004378	Cellular retinoic acid–binding protein 1 (CRABP1)	0.37
NM_001998	Fibulin 2	0.38
NM_001839	Calponin 3, acidic	0.38
NM_001183	ATPase, H+ transporting, lysosomal, subunit 1	0.39

Gene expression levels are expressed as means of fold-change, which is calculated by dividing the signals of each ALS sample by those of control samples, in the five patients with ALS.
ALS = amyotrophic lateral sclerosis.

bridization on selected genes. The mRNAs for acetyl-CoA transporter, KIAA0231, and EGR3 were localized in the remaining motor neurons (Fig 4). Spinal motor neurons overexpressed acetyl-CoA transporter and KIAA0231 in ALS, whereas EGR3 was underexpressed. Moreover, TrkC, CRABP1, Bak, and dynactin 1 gene expression was found in motor neurons, and those signals were reduced in ALS. DR5 signals were increased in motor neurons in ALS. Cyclin C signals with punctate immunoreactivity were increased in the cytoplasm as well as in nuclei in ALS motor neurons. The nuclear staining of motor neurons for cyclin C was more prominent in ALS compared with controls.

Discussion

Although reports about differential gene expression using the postmortem spinal cords, including those of patients with ALS, have been published,[26,27] the precise gene expression profiles of the degenerating motor neurons themselves have remained to be elucidated. Laser-captured dissection of motor neurons and subsequent microarray analysis are the most appropriate approaches to understanding the motor neuron–specific gene expression profile related to the motor neuron degeneration process in sporadic ALS, because these approaches eliminate bias of motor neuron loss, reactive astroglial proliferation, and other cellular reactions. Indeed, serine kinase has been reported to be underexpressed in ALS spinal cord gray matter,[27] but this study showed it was overexpressed in isolated motor neurons, suggesting that the reported underexpression in whole gray matter was influenced by the decreased motor neuron population. In contrast, cathepsin D expression was downregulated in the ALS motor neurons in this study, whereas it was increased in spinal cord gray matter in a previous report,[27] indicating its upregulation in glial cells. In addition, clustering analyses showed that the gene expression profile in the spinal motor neurons was substantially different from that in the whole homogenates of spinal ventral horn gray matter.

The overall microarray analysis using spinal ventral horn homogenates showed gene expression changes in less than 1% of genes examined with more genes showing increased than decreased expression. On the other hand, the motor neuron–specific microarray analysis

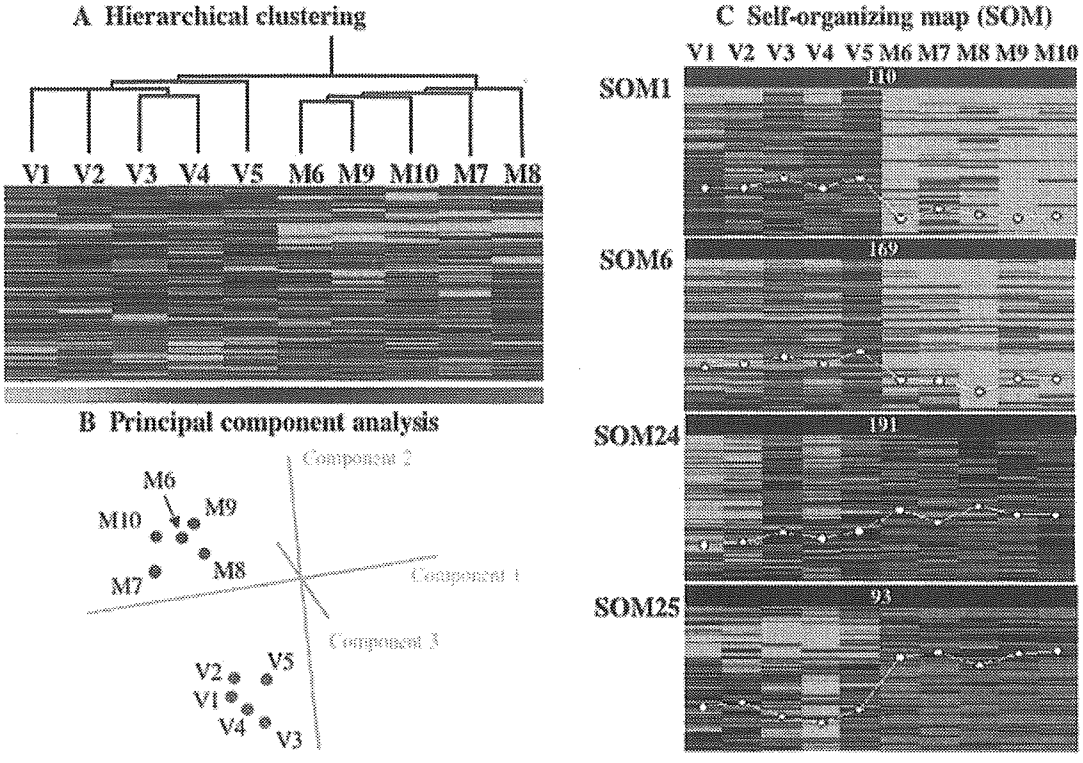

Fig 2. Clustering of gene expression in spinal motor neurons and spinal ventral horns. (A) Hierarchical clustering of gene expression in spinal motor neurons and ventral horns. The dendrogram was produced by hierarchical clustering of relative expression levels of 4,845 genes (rows) in five spinal homogenate and five motor neuron samples (columns) in making a total of 48,450 data points. Visual representation is shown with green representing downregulated (<0.44), black representing intermediate, and red representing upregulated (>2.28). The hierarchical clustering successfully detects two large clusters of amyotrophic lateral sclerosis (ALS), discriminating between spinal homogenates of ventral horns (samples V1 [ALS1], V2 [ALS10], V3 [ALS3], V4 [ALS14], and V5 [ALS13]) and motor neurons (samples M6 [ALS1], M7 [ALS10], M8 [ALS14], M9 [ALS11], and M10 [ALS7]), with a correlation coefficient of 0.446 at the branching point. (B) Principal component analysis of spinal motor neurons and ventral horns. Principal component analysis by six components for the 4,845 genes shows two main clusters consisting of spinal motor neurons (M6–10) and homogenates (V1–5). The number of patients corresponds to those in the dendrogram. (C) Self-organizing map (SOM) analysis of spinal motor neurons and ventral horns. The 4,845 genes are grouped into 25 clusters, the optimal size of which is calculated from gap statistics analysis. In SOM1 and SOM6, most genes are downregulated and in SOM24 and SOM25 the majority of genes are upregulated commonly in isolated motor neurons of five cases (M6–10). The numbers of genes are given at the top, and selected genes are listed for clusters 1, 6, 24, and 25 in Table 6.

showed that the proportion of significantly downregulated genes was 3% of the examined genes, whereas that of upregulated genes was one third of the downregulated genes. Moreover, the genes found to be downregulated specifically in motor neurons were not found to be downregulated in ventral horns, except for three genes with high expression levels. These results strongly support the notion that microarray analysis of laser-captured isolated spinal motor neurons has an advantage especially for the detection of motor neuron–specific downregulated transcripts.

In the differentially expressed genes, cell death–associated genes and genes related to cell signaling were characteristically upregulated in ALS motor neurons, whereas the genes categorized into cytoskeleton and transcription were downregulated. In the prominently altered genes of interest related to the cell death pathway, acetyl-coenzyme A transporter, which has been cloned and shown to encode a protein with multitransmembranous spanning domains,[28] was overexpressed in ALS motor neurons. Acetyl-CoA transporter functions as a cofactor for acetylation of gangliosides as well as vesicular transport of acetylcholine, which is synthesized from acetyl-CoA and choline. Acetylation has been documented to suppress proapoptotic activity of GD3 ganglioside, which increased in ALS neural tissues, as previously shown.[29,30] These results suggest that enhanced expression of acetyl-CoA transporter may be related to the antiapoptotic mechanism for cholinergic motor neuron degeneration in ALS.

Table 6. Selected Genes Characterized by SOM (select each 15)

GeneBank	Gene Name	Fold Change (ALS/control)
SOM1/6: genes downregulated in ALS motor neurons		
NM_002695	Polymerase (RNA) II (DNA directed) polypeptide E (25kD)	0.20
M24857	Retinoic acid receptor gamma 1 (RAR-γ 1)	0.20
NM_002375	Microtubule-associated protein 4	0.20
NM_001651	Aquaporin 5	0.21
NM_003178	Synapsin II	0.22
NM_004624	Vasoactive intestinal peptide receptor 1	0.23
NM_001740	Calbindin 2, (29kD, calretinin)	0.24
M73812	G1/S-specific cyclin E (CCNE)	0.25
NM_003206	Transcription factor 21	0.25
NM_004082	Dynactin 1 (p150)	0.30
U05012	TRK-C; NT-3 growth factor receptor precursor	0.31
NM_003632	Contactin associated protein 1	0.32
NM_005910	Microtubule-associated protein tau	0.49
NM_002373	Microtubule-associated protein 1A	0.51
NM_002442	Musashi (Drosophila) homolog 1	0.52
SOM24/25: genes upregulated in ALS motor neurons		
M60718	Hepatocyte growth factor (HGF)	3.42
L20814	Glutamate receptor subunit 2 (GLUR-2)	3.34
K02268	β-neoendorphin-dynorphin precursor	3.13
L19063	Glial cell line–derived neurotropic factor (GDNF)	3.08
NM_005543	Insulin-like 3	2.79
J04088	DNA topoisomerase II alpha (TOP2A)	2.58
M22489	Bone morphogenetic protein 2A (BMP2A)	2.57
U51004	Hint protein; protein kinase C inhibitor	2.26
M87507	Caspase 1, interleukin-1 β convertase precursor	2.21
NM_006196	Poly(rC)-binding protein 1	2.16
L29511	Growth factor receptor–bound protein 2	2.04
U78798	TRAF6	1.98
NM_001229	Caspase 9, apoptosis-related cysteine protease	1.89
U84388	Caspase and rip adaptor with death domain (CRADD)	1.83
U13737	Caspase-3	1.77

Gene expression levels are expressed as means of fold-change, which is calculated by dividing the signals of each ALS sample by those of control samples, in the five patients with ALS. Genes listed in Tables 2 and 3 are excluded.
SOM = self-organizing map.

KIAA0231 was one of the mostly overexpressed genes in ALS motor neurons, but the function of this gene product is not known.

In the greatly downregulated genes of interest related to transcription, EGR3, whose expression was remarkably reduced in motor neurons of ALS, is a zinc-finger immediate-early transcription factor that is important for neurotrophin-3 (NT-3) regulation. It is known that EGR3 knockout mice develop gait ataxia, scoliosis, resting tremors, and ptosis due to the degeneration of muscle spindles, through disruption of NT-3 regulation.[31] In ALS motor neurons, TrkC receptor for NT-3 was underexpressed, whereas NT-3 expression was not changed. The finding about TrkC-null mutant and NT-3–null mutant mice show that NT-3-TrkC signaling is required to maintain Ia afferent central synapses of DRG neurons.[32] The marked downregulation of EGR3 in spinal motor neurons may disrupt sensory-motor connections by decreasing NT-3-TrkC signaling, resulting in motor neuron degeneration.

For neurotrophic support for ALS motor neurons, this study showed the overexpression of CNTF, GDNF, and HGF involved in the functional category of cell signaling, suggesting that these neurotrophic factors would be secondarily and compensatorily upregulated after motor neuron degeneration. Indeed, GDNF expression has been reported to increase in the spinal cords and decrease in the muscles of sporadic ALS patients.[33] In contrast with these neurotrophic factors, midkine was one of the significantly downregulated neurotrophic factors. Because midkine plays important roles in promotion of neuronal survival as well as modulation of neuromuscular junctions,[34] its underexpression may be related to motor neuron degeneration. In addition, the gene expression of vascular endothelial growth factor, which has been identified as a critical factor for motor neuron degeneration,[35–37] did not change significantly in gene expression in this study. SOD1 gene expression was not altered in spinal motor neurons and ventral horns. Moreover, the gene expres-

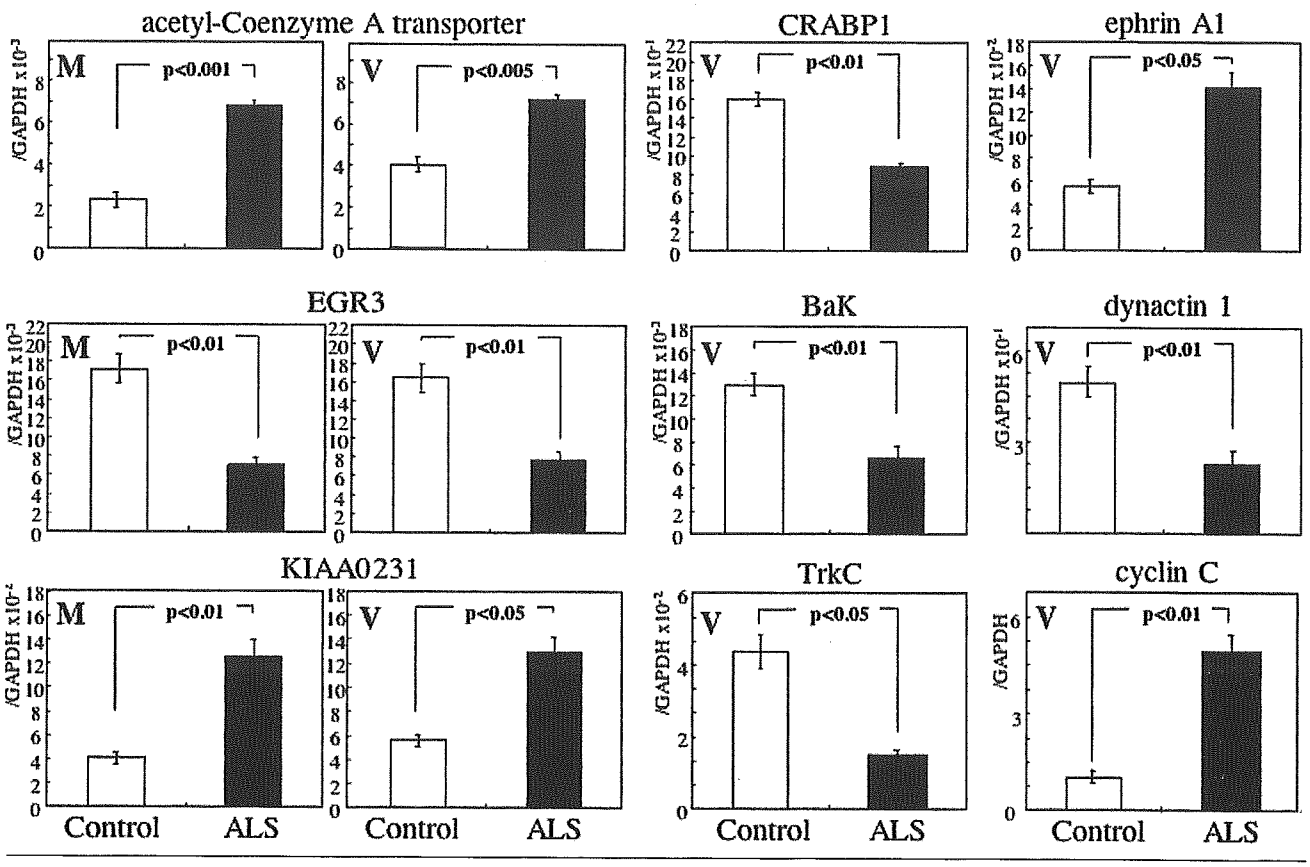

Fig 3. Quantitative real-time reverse transcription polymerase chain reaction verification of the selected genes. Expression levels of acetyl-coenzyme A transporter, EGR3, KIAA0231, CRABP1, Bak, TrkC, ephrin A1, cyclin C, dynactin 1, and GAPDH were measured using spinal motor neurons (M) and ventral horns (V), and those of the target genes were normalized against the GAPDH level. The relative expression levels are expressed as mean ± standard error for 13 amyotrophic lateral sclerosis (ALS) cases and 11 controls. Gene names (Genebank accession number), primers and probe sequences (forward primer, reverse primer, and TaqMan probe; 5' to 3' sequence) were as follows: [acetyl-CoA transporter: D88152] (GGGTTACTTTTTGGGCAATG, AACGATTCCTCTGGGTTGAG, FAM-TTGGCCCTTGAATCTGCCGA-TAMRA); [Bak: NM_001188] (CTGGAAGATCAGCACCCTAAG, CCCCTCTCCTAGTAGGTCCTG, FAM-TGCTCCCATTCCTCCCTCCG-TAMRA); [CRABP1: NM_004378] (TGCAGGAGTTTAGCCACTTG, CTCACGGGTCCAGTAGGTTT, FAM- TGAGAACAAGATCCACTGCACCCA-TAMRA); [cyclin C: M74091] (TGAGCAGTGGAAGAATTTCG, ACCCTGCTCTCCTTCACTGT, FAM- TGCCAAAACCAAAACCACCTCCA-TAMRA); [dynactin 1: NM_004082] (ATGTGAATCGGGAACTGACA, GGGCCTTAGTCTCAGCAAAC, FAM- TGGAGAGGCAACAGCAGCCAC-TAMRA); [EGR3: NM_004430] (CTTCCCCATGATTCCTGACT, TTGAATGCCTTGATGGTCTC, FAM-TTCCAGGGCATGGACCCCAT-TAMRA); [ephrin A1: M57730] (GGCAAGGAGTTCAAAGAAGG, TCACCTTCAACCTCAAGCAG, FAM- CCATCCACCAGCATGAAGACCG-TAMRA); [GAPDH: NM_002046] (TCAAGAAGGTGGTGAAGCAG, GGTGTCGCTGTTGAAGTCAG, FAM-CCTCAAGGGCATCCTGGGCT-TAMRA); [KIAA0231: D86984] (CAACGGTCTTCCAGACAATG, GAGGTTGACCAGCTGTGAGA, FAM-TCCCAGAGGTGAAGCTGCCCTCTAMRA); and [TrkC: U05012] (TGAGAACCCCCAGTACTTCC, TCAGCACGATGTCTCTCCTC, FAM-CTGCCACAAGCCGGACACGT-TAMRA).

sion level of GluR2 was upregulated, as shown by its classification in SOM25, but the expression of its editing enzyme (adenosine deaminase, RNA-specific, 2; ADAR2) was not altered in this study, although the editing efficiency of GluR2 mRNA has been demonstrated to be low in spinal motor neurons of ALS.[38]

Genes subject to transcriptional regulation constitute a crucial part of the whole human genome as demonstrated by human genome projects.[39] In addition to the gene expression of EGR3, the gene expression of retinoic acid receptor α and γ together with cellular retinoic acid–binding protein 1 (CRABP1), and Musashi 1, all of which are known to be inducers of neuronal differentiation,[40,41] was downregulated in spinal motor neurons of ALS. The dysregulation of retinoid receptor and retinol binding protein has been reported in the postmortem spinal cords of ALS and SOD1 mutant mice.[17,26] These interesting results imply the potential involvement of the differentiation signals in maintaining motor neuron integrity, which